Shape and Stress Analysis of Offset CRTS Reflectors

C.Y. Lai and S. Pellegrino

CUED/D-STRUCT/TR177(revised)

European Space Agency Contractor Report

The work presented in this report was carried out under an ESA contract.

Responsibility for its contents resides with the authors.

ESA Study Manager: W.J. Rits

ESTEC Contract no. 11936/96/NL/FG

Release date: 11 January 1999

Revised edition: 15 March 2001

Abstract

A new concept for multi-purpose deployable membrane reflectors is being developed by the European Space Agency; it is known as the *Collapsible Rib-Tensioned Surface (CRTS)* reflector. Prior to the study presented herein, there was concern over the applicability of the CRTS concept to offset reflectors. It was thought that setting up a prestressed membrane with asymmetric shape may be possible only with very stiff ribs.

It is shown in the report that CRTS reflectors with offset configuration are feasible, and extensive sets of results are presented to aid the design of future reflectors. Although the use of stiff ribs is still an option, the report presents two different ways of designing offset reflectors whose membranes are properly stressed and yet apply only in-plane loads on the ribs. Three different configurations of offset reflectors are introduced, whose rms errors are comparable but whose associated prestress distributions are different. It is found that one of these configurations can be used to produce reflectors with conventional offset shapes and prestress distributions that should be able to avoid the formation of wrinkles in the membrane. Another configuration produces prestress distributions as good as those previously obtained for symmetric reflectors, but requires a non-standard shape of the reflective surface.

A simple and effective way of determining prestress distributions that are approximately in equilibrium is developed, which can be used in the design of reflectors of general shape.

Contents

List of Tables

List of Figures

Chapter 1

Introduction

1.1 CRTS Reflectors

A new concept for multi-purpose deployable membrane reflectors is being developed by the European Space Agency (Rits 1996); it is known as the *Collapsible Rib-Tensioned Surface (CRTS)* reflector.

A CRTS reflector consists of three main parts. A central expandable hub, n thin-walled foldable ribs connected radially to the hub, and a precision shaped membrane that is supported and tensioned by the ribs. During deployment the radius of the hub is at its minimum, so that the ribs can deploy the membrane without having to prestress it at the same time. Once the membrane has been fully deployed, the hub is expanded, thus pushing outwards the ribs. This has the effect of applying a state of prestress to the membrane, which sets it into its intended shape.

This report is part of a series of studies of CRTS reflector technologies that are being carried out in the Deployable Structures Laboratory at the University of Cambridge. Previous studies in the series have dealt with:

- the behaviour of a straight rib when it is folded (Fischer 1994);
- the packaging of a CRTS reflector (You and Pellegrino 1994);
- the prestress of the membrane and the associated shape of the reflector (Lai, You and Pellegrino 1997);
- the deployment of straight ribs (Seffen and Pellegrino 1999); and
- the deployment of curved ribs (Seffen, You and Pellegrino 1997).

The studies listed above were mainly concerned with axi-symmetric reflectors, i.e. reflectors with identical gores. The present report deals with offset configuration reflectors, which are likely to be the preferred choice for communication applications.

1.2 Overview of Axi-symmetric Reflectors

This report extends and generalizes a previous study of symmetric reflectors by Lai, You and Pellegrino (1997). That study defined three different surfaces that are relevant to the design of a CRTS reflector: the *reference surface*, the *equilibrium surface*, and the *actual surface*.

The reference surface is a cylindrical surface defined by the parabolic ribs of the reflector. This surface is the best possible shape, as to achieve it the prestress of the membrane has to be only in the hoop direction, which is not acceptable as it would lead to the formation of wrinkles. The equilibrium surface is a shape of the reflector in which an acceptable prestress distribution is in equilibrium. This surface is calculated from the initial configuration of the reflector, given an initial prestress distribution, by means of the force density method, see below. Finally, the actual surface is formed when the prestress distribution obtained for the equilibrium surface is applied to a flat gore, whose edges are shaped according to a special cutting pattern that is obtained by projecting the equilibrium surface onto a flat shape. This surface is the expected shape of the reflector, which can be compared with experimental results.

Lai, You and Pellegrino (1997) developed a method for determining the shape of an axi-symmetric reflector, for a given prestress distribution. The membrane is represented by a virtual, triangulated cable network, and the assigned prestress in the membrane is transformed into equivalent cable forces in the virtual cable network. Having computed the ratio between the internal force in each cable and its length (force density), the equilibrium equations of the virtual cable structure provide a linear system of equations that can be solved to find the nodal coordinates of the virtual cable network. Once the positions of these nodes are obtained, the shape of the membrane is defined.

The procedure for determining the equilibrium shape of a gore is as follows.

1. Divide the gore into a set of small triangular elements;
2. Assume a stress distribution, i.e. prescribe the values of the stress components in local coordinates σ_{xx}, σ_{yy} and τ_{xy} in each triangle;
3. Replace each triangle with three cables and compute the force densities in these cables;
4. Assemble the equilibrium equations for the virtual cable net;
5. Solve the equilibrium equations to find the nodal coordinates;
6. Calculate the stress components in each membrane element, using the newly obtained nodal coordinates with the updated value of $\triangle$[1].

   Check the accuracy of the solution. If it is not satisfied, return to step (3) and repeat;

[1] $\triangle$ is the element area.

7. Determine the rms error of the current equilibrium surface.

   If the rms error is not acceptable, modify the stress distribution in step (2) and repeat.

8. Check that in all elements the current principal stresses are both positive, or greater than a specified minimum value.

D (m)	Configuration	Reference surface	Equilibrium surface	Actual surface
1	6 ribs	3.0	3.5	3.5
	12 ribs	0.9	1.3	1.3
	24 ribs	0.2	0.4	0.4
3	6 ribs	8.8	10.5	10.5
	12 ribs	2.6	3.9	3.9
	24 ribs	0.7	1.2	1.2
5	6 ribs	14.7	17.5	17.5
	12 ribs	4.3	6.6	6.6
	24 ribs	1.1	2.0	2.0
10	6 ribs	29.3	35.1	35.1
	12 ribs	8.6	13.1	13.1
	24 ribs	2.2	3.9	4.1

Table 1.1: Area-weighted rms errors, in millimetres, of symmetric reflectors with $F/D = 0.78$.

Table 1.1 shows the achievable surface accuracy (*rms error*) of symmetric reflectors with a particular value of F/D. Further details on the analysis are given in Lai, You and Pellegrino (1997), where a similar table is available.

1.3 Layout of this Report

Chapters 2 and 3 present the theoretical background to the analysis of offset CRTS reflectors.

Chapter 2 deals with geometrical aspects, including the definition of the co-ordinates of a series of nodes that lie on each rib. Three different configurations of offset CRTS reflectors are introduced. The standard configuration has the hub centred on the axis of the circular cylinder that is normally used to define the shape of an offset reflector. The central hub configuration has the hub centre at the point obtained by projecting onto a tangent plane the centre of the ellipse obtained by intersecting the cylinder and the paraboloid. The circular configuration is such that the projection of the end points of the ribs onto the tangent plane lie on a circle.

Chapter 3 describes the two types of rib-membrane boundary conditions that have been employed and, a major point of difference between symmetric and offset reflectors, a strategy for setting up initial states of prestress of the membrane that are in equilibrium in two-dimensions, i.e. assuming the whole reflector to lie in the tangent plane. By using states of prestress that are obtained from this approach, one can avoid large geometric distortions or changes of prestress when the full three-dimensional equilibrium is considered. This is a way of keeping the form-finding process "under control". This approach has been found very effective in the design of reflectors based on the standard and central configurations, as guessing a "good" initial state of prestress is impossible for these configurations.

Chapter 4 compares different designs for a reflector with a diameter of 1.2 m and 8 ribs. Both standard and central hub configurations are considered using two different variants of the prestress strategy of Chapter 3, and both types of boundary conditions. It is concluded that the best results are obtained for the central hub configuration, using a prestress strategy that enforces at each gore-gore interface equilibrium in the direction orthogonal to each rib, but not in the parallel direction.

In Chapter 5 the approach selected in Chapter 4 is applied to the design of reflectors of four different diameters and with different numbers of ribs. Extensive sets of results are presented, for future reference.

Chapter 6 explores an alternative type of design, based on the circular configuration. In this design the tips of the ribs are not co-planar, as they would be in the standard and central hub configurations. It is shown that this approach produces more even prestress distributions with surface accuracies that are comparable to the best results achieved in Chapter 5. Surface accuracies of reflectors with four different focal length to diameter ratios are also presented.

Chapter 7 concludes the report.

Chapter 2

Geometry

2.1 Background

The geometry of an offset parabolic antenna is defined by considering a large *parent reflector* from which a smaller circular region on one side and beyond the center of the parent is used as the reflecting surface (Levy 1996). Typically, the subreflector is located between the centre of the parent and the nearest rim of the offset reflector. Figure 2.1 shows a three-dimensional view of the offset antenna with the parent paraboloid. To help visualize the shape of the offset reflector, a series of contour lines have been drawn; these lines are obtained by intersecting the paraboloid with a series of concentric circular cylinders, whose axis is parallel to the Z-axis and passes through point O. The outermost cylinder, which defines the edge of the offset reflector, has radius R_a and is at a distance A from the Z-axis. A well-known property of a paraboloid of revolution is that the intersection between it and a circular cylinder with axis parallel to the axis of the paraboloid is a plane ellipse (Levy, 1996, p.18).

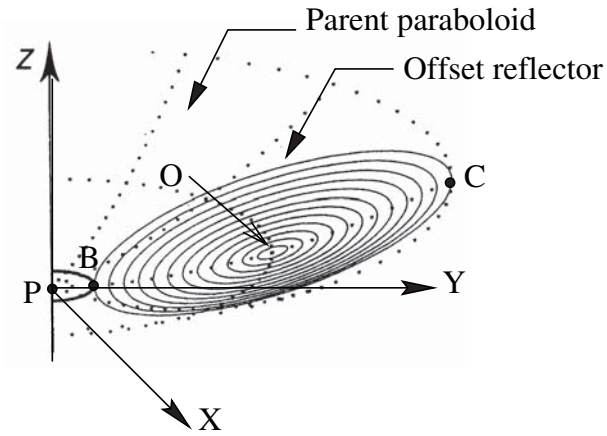

Figure 2.1: Three-dimensional view of offset reflector.

The equation of the parent paraboloid is

$$Z = \frac{X^2 + Y^2}{4F} \tag{2.1}$$

where F is the focal length of the paraboloid. The axes X, Y and Z are the principal axes of the parent paraboloid, see Fig. 2.1. Figure 2.2 defines two alternative sets of axes, whose origin O can be at any point on the centerline of the offset reflector, i.e. on the intersection between the parent paraboloid and the YZ plane. The position of O is determined by its Y-coordinate in the global coordinate system, Y_0.

The axes Y_1 and Z_1 are respectively parallel to Y and Z, but offset by Y_0 and Z_0, where $Z_0 = Y_0^2/4F$. The axes Y_L and Z_L relate to a local coordinate system in which Y_L is tangent to the centerline of the offset reflector. The angle between Y_L and Y_1 is ϕ_a, where $\phi_a = tan^{-1}(Y_0/2F)$. Note that the X-coordinates are the same for all three systems. Obviously

$$\begin{aligned} Y_1 &= Y - Y_0 \\ Z_1 &= Z - Z_0 \end{aligned} \tag{2.2}$$

Substituting equation 2.2 into equation 2.1 gives

$$Z_1 + Z_0 = \frac{1}{4F}[X^2 + (Y_1 + Y_0)^2] \tag{2.3}$$

Because it is more convenient to use local coordinates in the analysis of the reflector, the axes are rotated by an angle ϕ_a, giving

$$\begin{aligned} Y_1 &= cY_L - sZ_L \\ Z_1 &= sY_L + cZ_L \end{aligned} \tag{2.4}$$

where $c = \cos\phi_a$ and $s = \sin\phi_a$.
Substituting equation 2.4 into equation 2.3 gives the equation of the offset reflector in its local co-ordinate system X_L, Y_L, Z_L

$$sY_L + cZ_L + Z_0 = \frac{1}{4F}[X_L^2 + (cY_L - sZ_L + Y_0)^2] \tag{2.5}$$

Figure 2.3 shows two views of an offset reflector whose point O is such that its projection onto the Y-axis is half way between the projections of B and C, hence $Y_0 = A + R_a$. The first view, Fig 2.3(a), is along the Z-axis. The second view Fig 2.3(b), is along the Z_L-axis and hence it shows the projection of the reflector onto the X_LY_L plane.

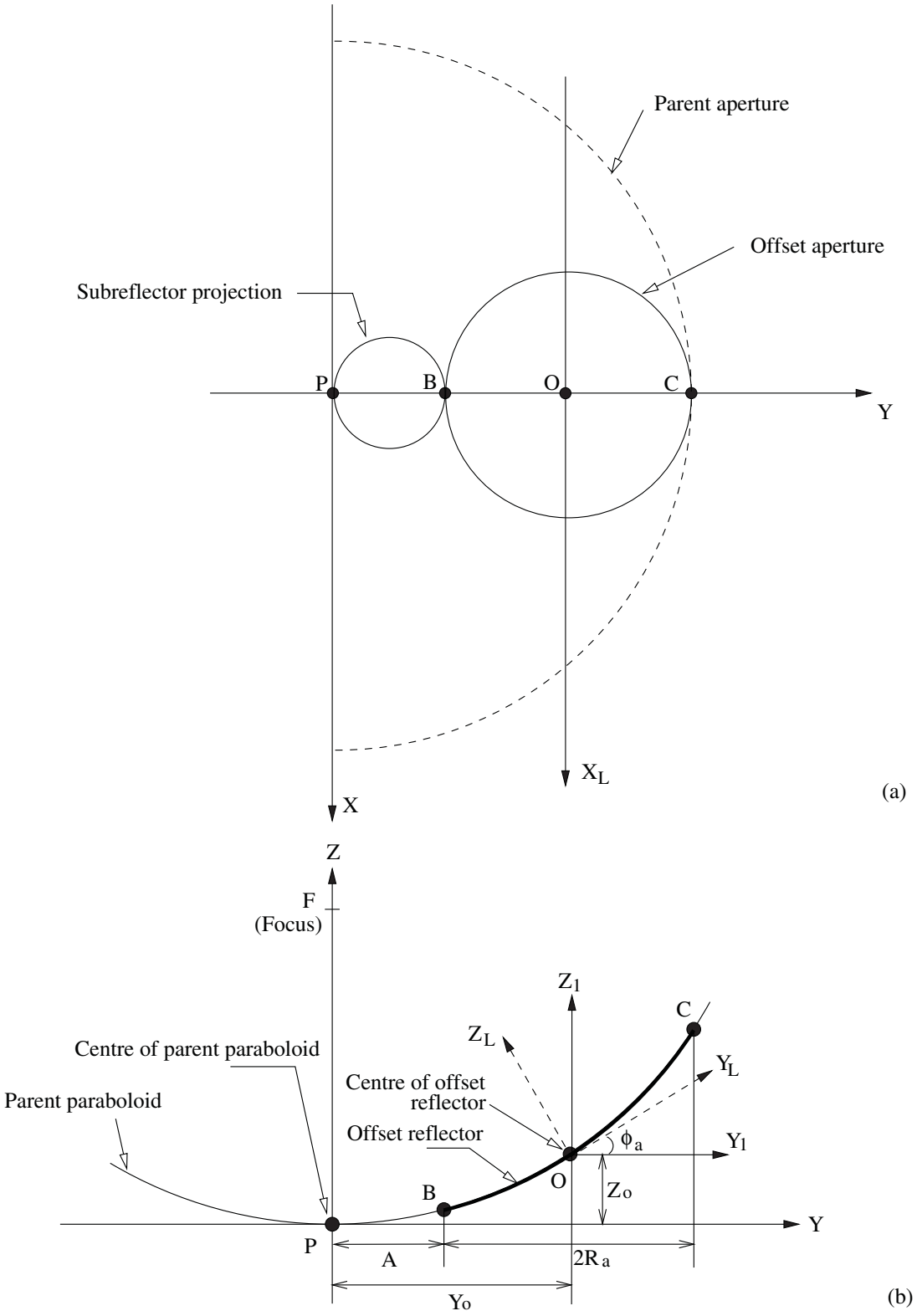

Figure 2.2: Definition of offset reflector from parent paraboloid: (a) projection onto XY plane; (b) intersection with ZY plane.

2.2 Standard Configuration

The first of the CRTS reflector configurations that will be considered has the centre of the hub at the point O, and the ribs lying in radial planes that are obtained by rotating the plane $Y_L Z_L$ about Z_L through angles that are integer multiples of $2\pi/N$, where N is the total number of ribs. So, for rib i

$$\alpha = 2i\pi/N \tag{2.6}$$

and α is the angle between the projection of rib i onto the $X_L Y_L$ plane and the Y_L axis.

The equation of this rib can then be obtained by intersecting the paraboloid with the radial plane, i.e. by eliminating either X_L or Y_L from Equation 2.5. Therefore, we substitute

$$\tan\alpha = \frac{X_L}{Y_L} \tag{2.7}$$

into Equation 2.5, which gives

$$\begin{aligned} &sY_L + cZ_L + Z_0 = \\ &\frac{1}{4F}\left[Y_L^2\tan^2\alpha + c^2Y_L^2 + s^2Z_L^2 + Y_0^2 - 2csY_LZ_L - 2sY_0Z_L + 2cY_0Y_L\right] \end{aligned} \tag{2.8}$$

To find Z_L we rearrange this equation into

$$\begin{aligned} &s^2Z_L^2 - \left[2csY_L + 2sY_0 + 4Fc\right]Z_L + \\ &\left[Y_L^2\tan^2\alpha + c^2Y_L^2 + Y_0^2 + 2cY_0Y_L - 4FsY_L - 4FZ_0\right] = 0 \end{aligned} \tag{2.9}$$

which is a quadratic equation whose solution is

$$\begin{aligned} Z_L = \quad & \frac{(2csY_L + 2sY_0 + 4Fc) \pm [(2csY_L + 2sY_0 + 4Fc)^2 -}{2s^2} \\ & \frac{4s^2(Y_L^2\tan^2\alpha + c^2Y_L^2 + Y_0^2 + 2cY_0Y_L - 4FsY_L - 4FZ_0)]^{1/2}}{2s^2} \end{aligned} \tag{2.10}$$

Of the two solutions, the one of interest is obtained for the $-$ sign, as the other one gives a much larger value of Z_L, corresponding to the intersection between the Z_L-axis and the left-hand side of the paraboloid.

Lastly, we need to determine the coordinates of the tip of rib i in the local coordinate system. To do this, we start in the coordinate system X_1, Y_1, Z_1, where the edge of the offset reflector is defined by a circular cylinder of radius R_a, see Fig. 2.3(a). In the X_1, Y_1, Z_1 coordinate system the coordinates of a

general point D on the edge of the offset reflector can be written, with the aid of Equation 2.3, in the form

$$\begin{aligned} X_{D1} &= R_a \sin\beta \\ Y_{D1} &= R_a \cos\beta \\ Z_{D1} &= \frac{1}{4F}[X_{D1}^2 + (Y_{D1} + Y_0)^2] - Z_0 \end{aligned} \tag{2.11}$$

The particular value of β that is required for point D to be at the tip of rib i is such that the coordinates of D in the X_L, Y_L, Z_L coordinate system, which are obtained from the inverse of Equation 2.4

$$\begin{aligned} X_{DL} &= X_{D1} \\ Y_{DL} &= cY_{D1} + sZ_{D1} \\ Z_{DL} &= -sY_{D1} + cZ_{D1} \end{aligned} \tag{2.12}$$

satisfy the condition

$$\tan\alpha = X_{DL}/Y_{DL} \tag{2.13}$$

for α given by Equation 2.6. Once the correct value of β has been found by an iterative process, the projected length R of rib i onto the XY_L plane is given by

$$R = Y_{DL}/\cos\alpha \tag{2.14}$$

In the reflector configuration that has been considered in this section, the hub of the reflector —which coincides with point O— was such that its projection onto the Y-axis was half-way between the projections of points B and C. This configuration of the reflector will be called the *standard configuration* of the reflector, because this position of point O is the normal choice for the local coordinate system of a standard offset reflector (Levy, 1996).

2.3 Central Hub Configuration

A second configuration of the CRTS reflector that will be considered has point O half-way between the projections onto the Y_L axis of points B and C. This configuration will be called the *central hub configuration.*

If we consider, as before, a series of circular cylinders to visualize the surface, the innermost cylinder has its axis through the new point O, whereas the outermost will be unchanged from that considered earlier. Therefore, these cylinders are no longer co-axial, as it is clear from Fig. 2.4(a). However, in the projection onto the X_LY_L plane, Fig. 2.4(b), the ellipses are now concentric.

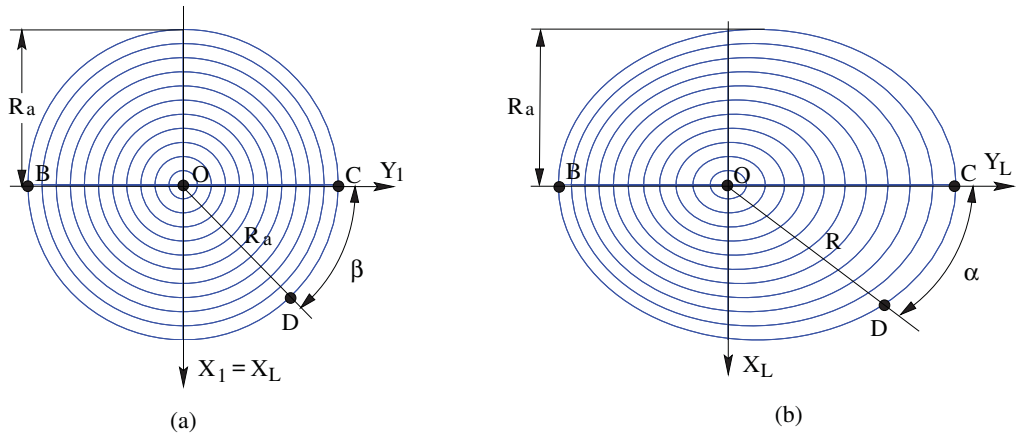

Figure 2.3: Projections of standard configuration onto (a) global plane; (b) local plane. Each line represents the intersection between the paraboloid and a circular cylinder with axis along Z_1.

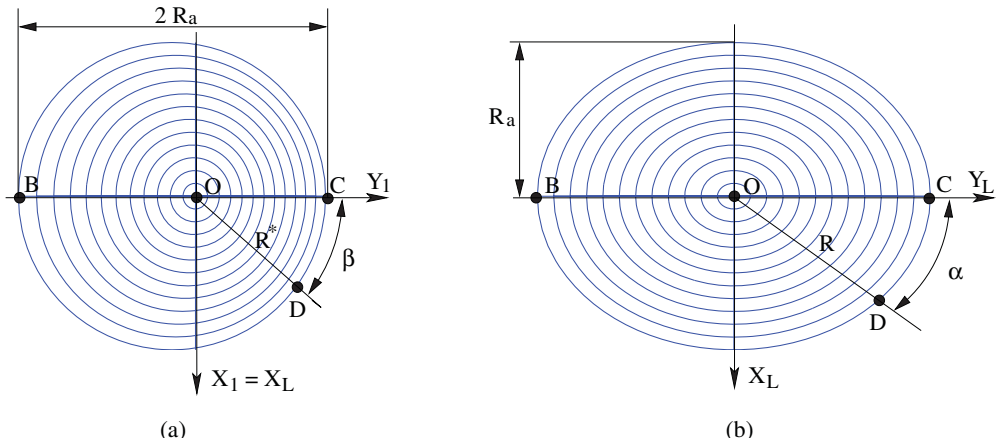

Figure 2.4: Projections of central hub configuration onto (a) global plane; (b) local plane.

An advantage of the central hub configuration is that, because its $X_L Y_L$ projection has two axes of symmetry instead of one only, it is possible to achieve a better prestress distribution, as it will be shown in Chapter 2.

To define this central hub configuration we need to find the value of Y_0 such that the Y_L coordinates of points B and C are equal and opposite, which means

$$Y_{BL} + Y_{CL} = 0 \tag{2.15}$$

Writing the second of the coordinate transformations in Equation 2.12 for point B, and substituting into Equation 2.2

$$Y_{BL} = cY_{B1} + sZ_{B1} = \cos\phi_a(Y_B - Y_0) + \sin\phi_a(Z_B - Z_0) \tag{2.16}$$

Then we substitute

$$\begin{aligned} \phi_a &= tan^{-1}\frac{Y_0}{2F} \\ Y_B &= A \\ Z_B - Z_0 &= \frac{A^2 - Y_0^2}{4F} \end{aligned}$$

into Equation 2.16, giving

$$Y_{BL} = \cos\left(\tan^{-1}\frac{Y_0}{2F}\right)(A - Y_0) + \sin\left(\tan^{-1}\frac{Y_0}{2F}\right)\frac{A^2 - Y_0^2}{4F} \tag{2.17}$$

In a similar way we find, for point C

$$Y_{CL} = \cos\left(\tan^{-1}\frac{Y_0}{2F}\right)(2R_a + A - Y_0) + \sin\left(\tan^{-1}\frac{Y_0}{2F}\right)\frac{(2R_a + A)^2 - Y_0^2}{4F} \tag{2.18}$$

Substituting Equations 2.17-2.18 into Equation 2.15 we obtain an equation in Y_0, which can be solved numerically. The value of Y_0 determines the position of the hub of the reflector.

Next, we need to determine the coordinates of the tip of each rib. This is done in the same way as for the normal hub configuration, but Fig. 2.4 shows that this time we need to use R^*, instead of R_a, in Equation 2.11. Applying the sine rule to $\triangle OQD$, see Figure 2.5 one obtains

$$R^* = \frac{R_a \sin\beta_1}{\sin(180^0 - \beta)} \tag{2.19}$$

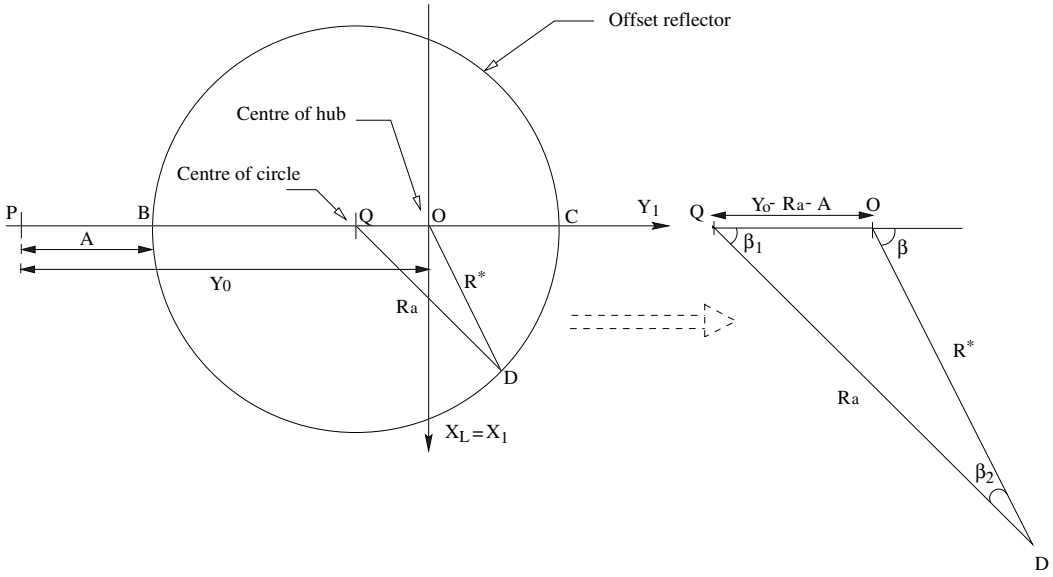

Figure 2.5: Hub position in CRTS reflector with central hub. The edge of the reflector is defined by the intersection between the $X_L Y_1$ plane and a cylinder of radius R_a.

2.4 Circular Configuration

The third configuration of the CRTS reflector that will be considered is such that its projection onto the local plane, defined by the axes X_L and Y_L is a circle, instead of an ellipse.

The geometry of the circular configuration is defined in a way similar to the central hub configuration, but now the radius of the projection onto the local $X_L Y_L$ is known: $R = R_a$. The only unknown is Y_0, which is found as follows.

Consider point B in Figure 2.2; an expression for Y_{BL} is given by Equation 2.16,

$$Y_{BL} = cY_{B1} + sZ_{B1} = \cos\phi_a(Y_B - Y_0) + \sin\phi_a(Z_B - Z_0) \qquad (2.20)$$

Here, $Y_{BL} = -R_a$, and hence Equation 2.20 can be solved for the unknown Y_0. Then the coordinates of the end point of each rib are determined in exactly the same way as for the previous configurations.

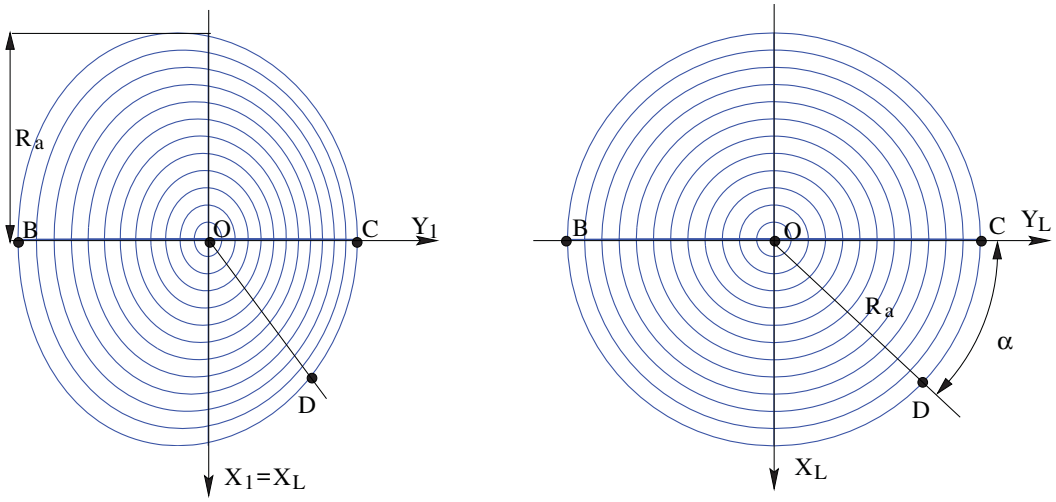

Figure 2.6: Projections of circular configuration onto (a) global plane; (b) local plane. Each line represents the intersection between the paraboloid and a circular cylinder with axis along Z_L.

Chapter 3

Computational Analysis

The main structure of the analysis of an offset reflector is very similar to a symmetric reflector: given an initial configuration of the reflector, with its nodal coordinates, boundary conditions, and initial prestress distribution, the final equilibrium geometry of the membrane is computed using the force density method. Details can be found in the previous report (Lai, You and Pellegrino 1997).

The offset reflector surface is divided into a number of gores, attached to ribs that are modelled as rigid in the formfinding analysis. Once the forces applied by the membrane onto the ribs are known, the elastic compliance of the ribs is considered, to compute their initial, unstressed shape. The number of ribs depends upon the size and surface accuracy required from the antenna surface, and the ribs are equally spaced, for simplicity.

An offset reflector has only one plane of symmetry, $Y_L Z_L$, and therefore half of the reflector needs to be considered in the analysis, instead of only one gore as in the symmetric case. The equilibrium shape of the membrane depends upon the initial prestress distribution that is assigned for it, and this distribution has to vary from one gore to the next as the shape of each gore is different.

A major challenge is to obtain an initial prestess distribution such that the subsequent form-finding analysis will produce only minor distortions. Initially, a trial-and-error approach was attempted, but it had to be abandoned, as avoiding significant distortion during form-finding proved impossible. The alternative approach that was developed, and that will be presented here, is based on initial prestress distributions that are approximately in equilibrium, and hence require only a small adjustment of the shape of the surface.

Another important aspect of the form-finding analysis of offset reflectors is that, because adjacent gores are stressed differently, it cannot be guaranteed — in general— that the forces applied to the rib will lie within the plane of the rib. On the other hand, subjecting the lightweight ribs to out-of-plane loading would cause them to bend and twist in a complex way, which is undesirable. This problem will be addressed in two different ways; first, by considering initial prestress distributions that do not apply any out-of-plane loading on the ribs and, second, by implementing a rib-membrane boundary condition which allows the membrane to slide with respect to the rib, so that during form-finding no

out-of-plane forces are applied to the rib.

3.1 Initial Mesh

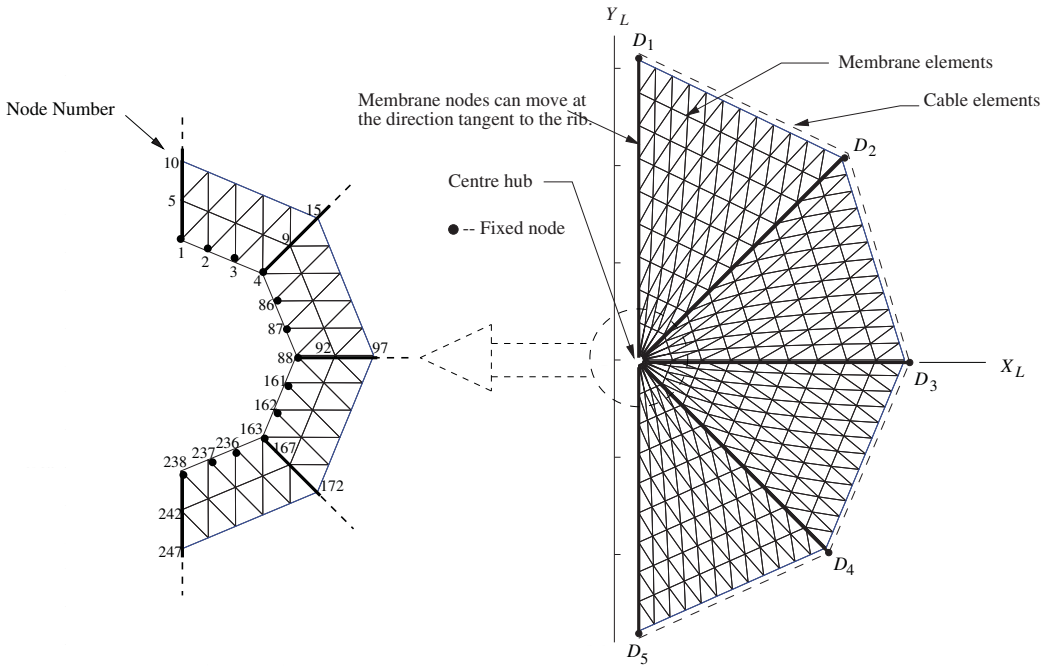

Figure 3.1: Example of initial mesh, plan view.

The coordinate system used for the form-finding analysis is the local coordinate system O, X_L, Y_L, Z_L defined in Section 2.1 and Fig. 2.2. Hence, the coordinates of the centre of the hub, O, are $(0, 0, 0)$.

Figure 3.1 shows the initial mesh, in plan view. There are two different types of elements in each gore: the membrane elements representing the surface and the cable elements representing the cord at the edge of the membrane. The orientation of the mesh, i.e. node and element numbering, is the same as that used for the symmetric reflector, to minimise changes in the computational analysis. However, as explained above, only half of the reflector is considered in the analysis, instead of a single gore.

The initial geometry of the reflector is defined as follows. First, the coordinates of the nodes lying on the ribs are defined. For rib i, the angle α_i with the Y_L axis and the coordinates of the tip node D_i are determined by the method of Section 2.1. Then, the coordinates of point H_i at the edge of the hub are determined: H_i is at a specified distance from O, which defines the value of X_{H_iL}, Y_{H_iL}. The Z_L coordinate is determined from Equation 2.10. Finally, a specified number of equally spaced nodes are defined by interpolation between Y_{H_iL} and Y_{D_iL}, and their Z_L coordinates are determined from Equation 2.10.

Once the rib nodes have been defined, all of the membrane nodes are defined: they lie on straight lines between corresponding nodes on two adjacent ribs, and hence their coordinates can be found by interpolation of the coordinates of the two rib nodes.

3.2 Boundary Conditions

All of the nodes are unconstrained, apart from the following: (i) the nodes at the interface with the hub are constrained in all three directions; (ii) the nodes at the interface with the ribs are either fixed, or allowed to slide in a direction parallel to the rib ($\parallel$), or to slide in a direction perpendicular to the plane containing the rib ($\perp$).

These boundary conditions are applied by modifying the equilibrium equations of the nodes involved. Recall that the membrane surface is represented by a set of triangular elements, and for each element we can write up to nine equilibrium equations

$$\mathbf{E} \begin{bmatrix} X_1 \\ Y_1 \\ Z_1 \\ X_2 \\ Y_2 \\ Z_2 \\ X_3 \\ Y_3 \\ Z_3 \end{bmatrix} = \begin{bmatrix} P_{1XL} \\ P_{1YL} \\ P_{1ZL} \\ P_{2XL} \\ P_{2YL} \\ P_{2ZL} \\ P_{3XL} \\ P_{3YL} \\ P_{3ZL} \end{bmatrix} \tag{3.1}$$

where $\mathbf{E}$ is the equilibrium matrix for the element, X, Y, Z are the coordinates of the nodes in the coordinate system O, X_L, Y_L, Z_L, and P_{iXL}, etc. are the external nodal force components on the node.

3.2.1 Fixed boundary

At a fully constrained node no equilibrium equations need to be considered, since the coordinates of the node are known and the reaction components applied to the nodes will equilibrate any unbalanced forces. Therefore, the size of the equilibrium matrix for an element with one or more constrained nodes will be appropriately reduced. The equilibrium equations for an element with one fixed node and two free nodes, as shown in Fig. 3.2, are

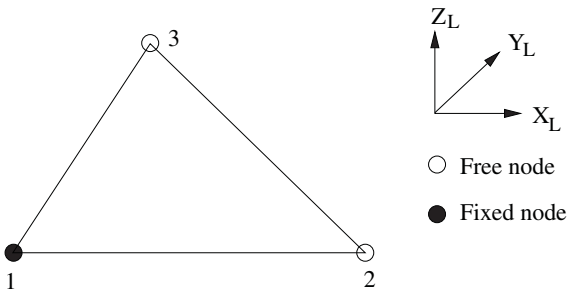

Figure 3.2: Triangular element with a fixed node.

$$\mathbf{E}^* \begin{bmatrix} X_2 \\ Y_2 \\ Z_2 \\ X_3 \\ Y_3 \\ Z_3 \end{bmatrix} = \begin{bmatrix} P^*_{2XL} \\ P^*_{2YL} \\ P^*_{2ZL} \\ P^*_{3XL} \\ P^*_{3YL} \\ P^*_{3ZL} \end{bmatrix} \tag{3.2}$$

where $\mathbf{E}^*$ is $\mathbf{E}_{(4-9,4-9)}$ and $\mathbf{P}^* = \mathbf{P} - \mathbf{E}_{(4-9,1-3)} \times [X_1, Y_1, Z_1]^T$.

3.2.2 Sliding boundary

Sliding boundary conditions are applied at the rib nodes, in order to control the reaction forces applied to the flexible ribs. Two different cases will be considered: (i) a rib node is free in the direction perpendicular to the plane of the rib, but is fully constrained in the plane of the rib, and (ii) a rib node is free to move in the direction of the local tangent to to the rib, but is constrained in two directions perpendicular to it. Both situations can be analysed as shown next.

Consider, for example, an element with two unconstrained nodes; node 1 is subject to a sliding boundary condition, Fig. 3.3. Let a be the direction along which sliding is permitted: b, c are two directions perpendicular to a. Let (a_X, a_Y, a_Z), etc. be the direction cosines of a, b, c along X_L, Y_L, Z_L.

The external force components on node 1 are transformed from the X_L, Y_L, Z_L system to a, b, c by the rotation matrix

$$\begin{bmatrix} P_{1XL} \\ P_{1YL} \\ P_{1ZL} \end{bmatrix} = \begin{bmatrix} a_X & b_X & c_X \\ a_Y & b_Y & c_Y \\ a_Z & b_Z & c_Z \end{bmatrix} \begin{bmatrix} P_{1a} \\ P_{1b} \\ P_{1c} \end{bmatrix} \tag{3.3}$$

Substituting Equation 3.3 into Equation 3.1, the first three rows of the equation become

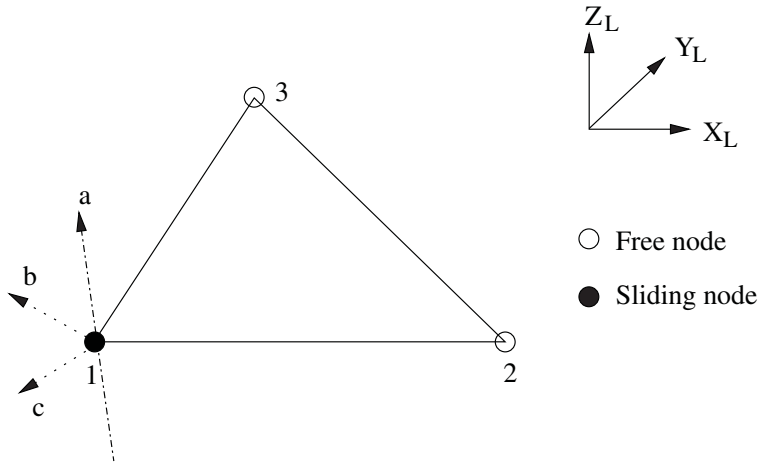

Figure 3.3: Element subject to sliding boundary condition.

$$\mathbf{E}\begin{bmatrix} X_1 \\ Y_1 \\ . \\ . \\ Z_3 \end{bmatrix} = \begin{bmatrix} a_X & b_X & c_X \\ a_Y & b_Y & c_Y \\ a_Z & b_Z & c_Z \end{bmatrix} \begin{bmatrix} P_{1a} \\ P_{1b} \\ P_{1c} \end{bmatrix} \tag{3.4}$$

Since the inverse of a rotation matrix is its transpose

$$\begin{bmatrix} a_X & a_Y & a_Z \\ b_X & b_Y & b_Z \\ c_X & c_Y & c_Z \end{bmatrix} \mathbf{E}\begin{bmatrix} X_1 \\ Y_1 \\ . \\ . \\ Z_3 \end{bmatrix} = \begin{bmatrix} P_{1a} \\ P_{1b} \\ P_{1c} \end{bmatrix} \tag{3.5}$$

Of these three equations, only the first one will be included in the set of equilibrium equations for the element, because equilibrium in the b and c directions is automatically satisfied, due to the existence of reaction forces. This would leave a total of seven equations in nine unknowns. However, node 1 is allowed to move only in the a-direction, starting from its initial coordinates $X_{1L}^0, Y_{1L}^0, Z_{1L}^0$. Therefore, its final coordinates can be expressed as

$$\begin{aligned} X_{1L} &= a_X\alpha + X_{1L}^0 \\ Y_{1L} &= a_Y\alpha + Y_{1L}^0 \\ Z_{1L} &= a_Z\alpha + Z_{1L}^0 \end{aligned} \tag{3.6}$$

and, substituting these expressions into Equation 3.5 we obtain

$$\mathbf{E}^* \begin{bmatrix} \alpha \\ . \\ . \\ . \\ Z_3 \end{bmatrix} = \begin{bmatrix} P^*_{1a} \\ P^*_{2X} \\ . \\ . \\ P^*_{3Z} \end{bmatrix} \tag{3.7}$$

3.3 Prestressing Strategy

In a symmetric CRTS reflector all gores are identical and equally prestressed, and hence no out-of-plane forces are applied on the ribs. Because an offset reflector is not axi-symmetric, the size, shape, and prestress of the gores that make up half of the reflector are different.

If it is assumed that the ribs are sufficiently stiff and strong that they can carry any out-of-plane forces, the rib nodes at the edge of each gore can be modelled as fully constrained, and the form-finding can be carried out for each gore independently. Considering this case in the analysis is straightforward, and the results that are obtained will be used as a reference.

In practice, the forces applied by the membrane to the flexible ribs have to be kept within the plane of curvature of the ribs, so that the longitudinal axis of each rib in the unstressed shape is a two-dimensional curve: this will make it a lot easier to manufacture the ribs. In this case, the form-finding analysis has to be done for half of the reflector and sliding boundary conditions have to be assumed. To avoid large shape distortions and severe changes of the stress distribution, the initial prestress distribution needs to be almost in equilibrium.

3.3.1 Computation of membrane prestress

We will consider only states of pre-stress where each gore is subject to uniform stress and the principal stress directions of gore i are aligned with the local x_i, y_i axes for the gore. The x_i-axis is parallel to the projection of D_iD_{i+1} onto the plane X_LY_L, and y_i is perpendicular to x_i. These principal stress components, multiplied by the thickness of the membrane are denoted by t_{xi} and t_{yi}.

The values of t_{xi} and t_{yi} will be required to satisfy equilibrium in the plane X_L, Y_L. It would be impossible to attempt to satisfy equilibrium also in the Z_L direction, as this can only be achieved when each gore takes a doubly curved shape.

Consider, for example, a standard configuration offset CRTS reflector with eight ribs, whose projections in X_L, Y_L plane are at 45° to each other. Figure 3.4 shows half of the projection, the symmetric half is not shown. From the centre of the ellipse, O, draw perpendicular lines to the cords D_1D_2, D_2D_3, etc. to define points H, J, etc. Clearly

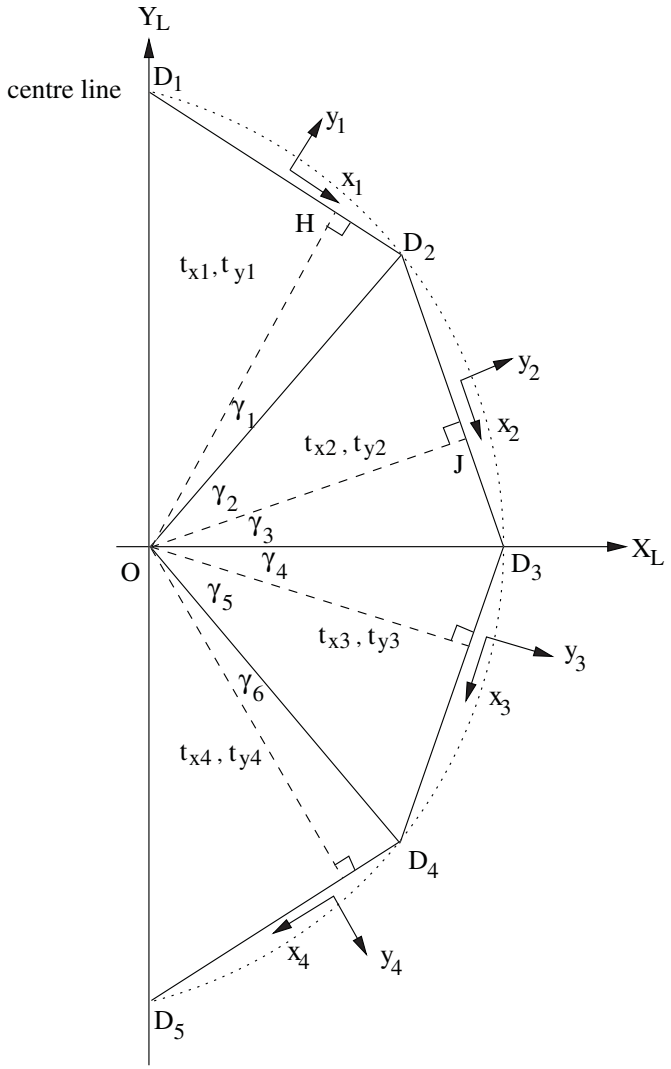

Figure 3.4: Projection of half of the reflector onto local X_L, Y_L plane.

$$\begin{aligned}\overline{OH} &= \overline{OD_2}\cos\gamma_1\\ \overline{OJ} &= \overline{OD_2}\cos\gamma_2\\ \overline{D_2H} &= \overline{OD_2}\sin\gamma_1\\ \overline{D_2J} &= \overline{OD_2}\sin\gamma_2\end{aligned}$$

Now consider a free body consisting of the projection onto the X_LY_L plane of membrane elements OD_2H and OD_2J, as shown in Figure 3.5. At this point we can take two different strategies: (i) we assume that rib OD_2 applies no external forces to this free body, or (ii) that it can only apply forces parallel to OD_2.

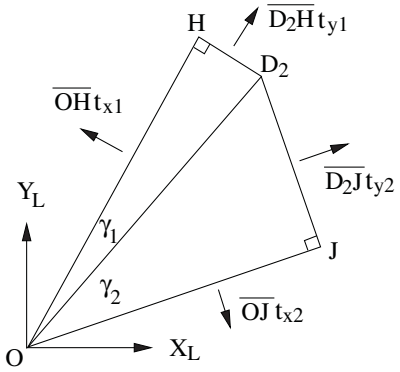

Figure 3.5: Free body diagram for membrane elements OD_2H and OD_2J.

With the **first strategy** we enforce equilibrium both in the direction parallel to OD_2 and orthogonal to it. Equilibrium in the direction orthogonal to OD_2 requires

$$\overline{OH}\cos\gamma_1 t_{x1} + \overline{D_2H}\sin\gamma_1 t_{y1} - \overline{OJ}\cos\gamma_2 t_{x2} - \overline{D_2J}\sin\gamma_2 t_{y2} = 0 \qquad (3.8)$$

Equilibrium in the direction parallel to OD_2 requires

$$\overline{OH}\sin\gamma_1 t_{x1} + \overline{D_2H}\cos\gamma_1 t_{y1} - \overline{OJ}\sin\gamma_2 t_{x2} - \overline{D_2J}\cos\gamma_2 t_{y2} = 0 \qquad (3.9)$$

In the example shown in Figure 3.4 eight unknown stress components need to be computed to completely define the initial state of prestress. By choosing any two of $t_{x1}, t_{y1}, t_{x2}, ...t_{y4}$ we can use Equations 3.8-3.9, written for the three ribs to determine the remaining six stress components.

In the **second strategy** we consider only equilibrium in the direction orthogonal to the ribs, and require the stresses t_{x1}, t_{x2}, etc. to be in equilibrium in these directions. We also require that the stresses t_{y1}, t_{y2}, etc. are independently in equilibrium in the direction perpendicular to the ribs. The reason for

doing this is to keep the "hoop" stress components —in the x_i direction— in the membrane separate from the "radial" component —in the y_i direction— to avoid that the higher radial stresses spill into the radial direction. Hence, we replace Equation 3.8 by the following two equations:

$$\begin{aligned} \overline{OH}\cos\gamma_1 t_{x1} - \overline{OJ}\cos\gamma_2 t_{x2} &= 0 \\ \overline{D_2H}\sin\gamma_1 t_{y1} - \overline{D_2J}\sin\gamma_2 t_{y2} &= 0 \end{aligned} \tag{3.10}$$

Once both stress components have been prescribed for one rib, all the others can be found from equations similar to the above.

Note that the first strategy assumes that the ribs apply no distributed forces to the membrane but, of course, a force will be applied by the edge cords to the tip of each rib. Also, distributed forces in the Z_L direction are required for equilibrium. In the second strategy each rib will be subject not only to tip forces and distributed forces in the Z_L direction, but also to distributed forces parallel to the rib. In practice these forces can be carried by a narrow strip of membrane in the vicinity of the rib, instead of being transmitted to the rib.

3.3.2 Computation of cord tensions

The out-of-straightness, or *sag* of the edge of the membrane is related by equilibrium to the prestress in the membrane and the tension in the edge cord. To avoid that the form-finding algorithm comes up with unrealistic shapes, we compute an approximate value for the tension cord that is required to produce an acceptable sag.

Consider Figure 3.6, which is assumed to be the equilibrium shape shown in Figure 3.4. It is assumed that the prestress distribution in the membrane has already been determined, as discussed in the previous sub-section, and that each cord has a symmetric shape and so the tangent at the centre point of cord i is parallel to x_i.

Now consider the two free bodies shown in Figure 3.7, obtained by considering half of a cord plus a piece of membrane with edges parallel to x_i and y_i. Note that T_i is the tension in the middle of cord i, and T_{xi}, T_{yi} are the x_i, y_i components of the tension in the cord at point D_2.

Taking moments about D_2 for the two bodies we obtain

$$T_1 s_1 - t_{x1} s_1^2/2 - t_{y1}\overline{D_1D_2}^2/8 = 0 \tag{3.11}$$

$$-T_2 s_2 + t_{x2} s_2^2/2 + t_{y2}\overline{D_2D_3}^2/8 = 0 \tag{3.12}$$

Resolving in the x_i, y_i directions the forces acting on each body

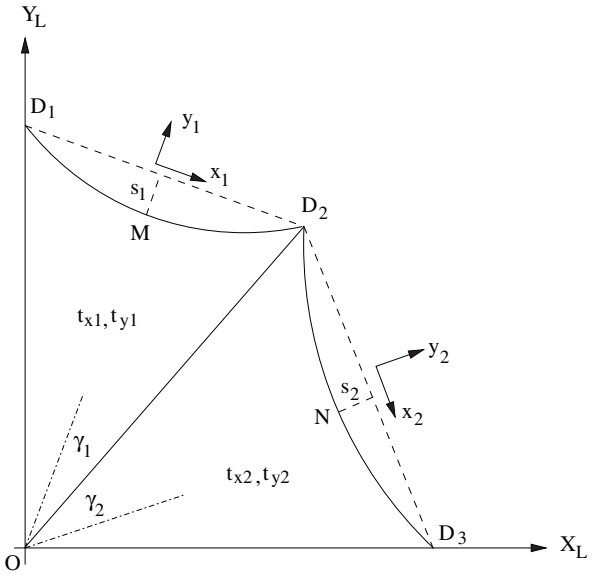

Figure 3.6: Shape of the edge cords, c.f. Fig. 3.4.

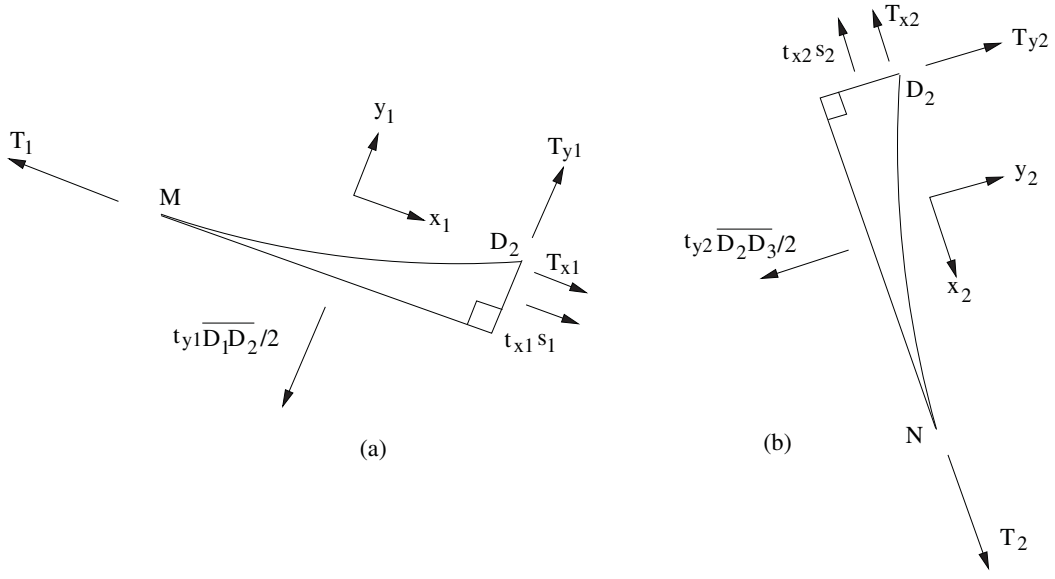

Figure 3.7: Free body diagrams for half cords and associated pieces of membrane.

$$\begin{aligned} T_{x1} &= T_1 - t_{x1}s_1 \\ T_{y1} &= t_{y1}\overline{D_1D_2}/2 \\ T_{x2} &= T_2 - t_{x2}s_2 \\ T_{y2} &= t_{y2}\overline{D_2D_3}/2 \end{aligned} \tag{3.13}$$

Next, consider the equilibrium of joint D_2, see Figure 3.8, subject to forces equal and opposite to T_{x1}, T_{y1}, and T_{x2}, T_{y2}, plus the axial and shear forces in the rib D_1D_2. For the shear force to be zero, the above four force components must be in equilibrium in the direction perpendicular to D_1D_2, thus

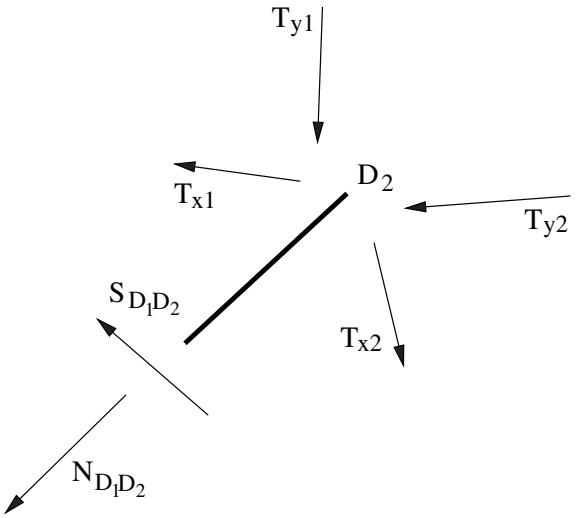

Figure 3.8: Free body diagram for joint D_2.

$$T_{x1}\cos\gamma_1 - T_{y1}\sin\gamma_1 - T_{x2}\cos\gamma_2 + T_{y2}\sin\gamma_2 = 0 \tag{3.14}$$

Substituting Equation 3.13 into Equation 3.14

$$(T_1 - t_{x1}s_1)\cos\gamma_1 - \frac{t_{y1}\overline{D_1D_2}}{2}\sin\gamma_1 - (T_2 - t_{x2}s_2)\cos\gamma_2 + \frac{t_{y2}\overline{D_2D_3}}{2}\sin\gamma_2 = 0 \tag{3.15}$$

Solving for T_2

$$T_2 = \frac{(T_1 - t_{x1}s_1)\cos\gamma_1 - (t_{y1}\overline{D_1D_2}/2)\sin\gamma_1 + (t_{y2}\overline{D_2D_3}/2)\sin\gamma_2}{\cos\gamma_2} + t_{x2}s_2 \tag{3.16}$$

Substituting into Equation 3.12

$$\frac{t_{x2}s_2^2}{2} = -\frac{(T_1 - t_{x1}s_1)\cos\gamma_1 - (t_{y1}\overline{D_1D_2}/2)\sin\gamma_1 + (t_{y2}\overline{D_2D_3}/2)\sin\gamma_2}{\cos\gamma_2}s_2 + \frac{t_{y2}\overline{D_2D_3}^2}{8} \tag{3.17}$$

With the above equations we can compute a set of cord tensions that will produce acceptable values of the sag. For the offset reflector, only one value can be chosen, i.e. either the sag or the tension in one cord; everything else follows from the above equations. The sequence of computations is as follows.

1. Assign value of sag of cord 1, s_1 (Values around $D/15$ are usually acceptable).
2. Compute central tension in cord 1, T_1, from Equation 3.11.
3. Compute sag of cord 2 from Equation 3.17.
4. Compute central tension in cord 2, T_2, from Equation 3.16.
5. If there are additional gores, the last two steps are repeated.

3.3.3 Examples

An offset reflector with aperture $D = 1.2$ m, offset $A = 0.2$ m, and 8 ribs was chosen for a preliminary analysis. The focal length of this reflector is 1 m, giving $F/D = 0.833$. The analytical model has 310 nodes, 540 membrane elements, 48 cable elements and 11 nodes are placed on each rib.

The two prestress stategies introduced in Section 3.3.1 give very different results, which means that the corresponding equilibrium shapes will also be different. Tables 3.1-3.4 show the initial stress distributions on the four gores, for two different sets of assigned stress components; these values are shown in **bold**. The prescribed value for the sag of cord 1 is $s_1 = D/15$. Both the standard configuration reflector and the central hub configuration of the reflector are considered.

	gore 1	gore 2	gore 3	gore 4
t_x (N/m)	**80**	**75**	76	75
t_y (N/m)	292	203	152	165
T (N)	123	126	127	126
t_x (N/m)	**80**	**80**	83	82
t_y (N/m)	238	158	112	125
T (N)	100	102	102	101
t_x (N/m)	**80**	**85**	90	88
t_y (N/m)	184	112	170	83
T (N)	78	78	76	77

Table 3.1: Initial prestress in standard configuration reflector, using prestress strategy 1. Assigned values shown in bold.

	gore 1	gore 2	gore 3	gore 4
t_x (N/m)	**80**	91	97	95
t_y (N/m)	**60**	29	19	21
T (N)	28	24	23	23
t_x (N/m)	**80**	91	97	95
t_y (N/m)	**80**	39	25	28
T (N)	36	32	31	31
t_x (N/m)	**80**	91	97	95
t_y (N/m)	**100**	49	31	36
T (N)	44	40	39	39

Table 3.2: Initial prestress in standard configuration reflector, using prestress strategy 2. Assigned values shown in bold.

	gore 1	gore 2	gore 3	gore 4
t_x (N/m)	**80**	**75**	75	80
t_y (N/m)	317	257	257	317
T (N)	120	122	122	120
t_x (N/m)	**80**	**80**	80	80
t_y (N/m)	221	171	171	221
T (N)	85	84	84	85
t_x (N/m)	**80**	**85**	85	80
t_y (N/m)	125	86	86	125
T (N)	49	47	47	49

Table 3.3: Initial prestress in central hub configuration reflector, using prestress strategy 1. Assigned values shown in bold.

	gore 1	gore 2	gore 3	gore 4
t_x (N/m)	**80**	86	86	80
t_y (N/m)	**60**	39	39	60
T (N)	25	23	23	25
t_x (N/m)	**80**	86	86	80
t_y (N/m)	**80**	52	52	80
T (N)	33	30	30	33
t_x (N/m)	**80**	86	86	80
t_y (N/m)	**100**	65	65	100
T (N)	40	37	37	40

Table 3.4: Initial prestress in central hub configuration reflector, using prestress strategy 2. Assigned values shown in bold.

Chapter 4

Analysis of 1.2 m Reflector

This chapter presents an extensive set of results for an eight-rib, 1.2 m diameter reflector. The reason why we have chosen this size and number of ribs is that they may be suitable for the design of a small-scale demonstrator. The geometry of the reflector is defined in Table 4.1. Two different configurations —standard and central hub— are analysed, for different prestress distributions and different types of boundary conditions. The rms accuracy of the reflector is estimated for each case that is considered, see Table 4.2 and 4.3, as well as the equilibrium prestress distribution, Table 4.4 and 4.5, in order to identify the approach that produces the best results. It is concluded that the best results are obtained for the central hub configuration reflector using prestress strategy 2 with the sliding $\perp$ boundary condition.

Diameter (D)	1.2 m
Focal length (F)	1 m
Offset (A)	0.2 m
Hub diameter	0.2 m
Number of ribs	8
F/D	0.833

Table 4.1: Geometry of 1.2 m reflector.

4.1 Reference surface

The concept of reference surface of a CRTS reflector was proposed for symmetric reflectors in our previous report (Lai, You, and Pellegrino 1997). Because the ribs of a symmetric reflector are identical, the reference surface for a gore is a cylindrical surface.

In an offset reflector the ribs are no longer identical, and hence it is impossible to form a cylindrical surface between them. In this case, the reference surface is defined as the surface obtained by connecting corresponding points on consecutive

ribs by means of straight lines. Note that the surface formed by these lines is a twisted surface and, because in general the ribs have different length, these lines do not lie in parallel planes.

Although it cannot be stated with certainty that the reference surface is the best achievable surface for an offset CRTS reflector, in practice it appears that this is so. In any case, it gives an easy-to-compute reference value of the accuracy achievable, as it will be shown, and it will be used as the initial geometry for our form-finding analysis. Figure 4.1 shows the initial meshes for offset reflectors with standard and central hub configuration, in plan view. The rms errors of these two reference surfaces are given in Table 4.2.

configuration	rms error
standard	3.2
central hub	3.2

Table 4.2: Rms error (mm) of reference surface.

The geometry of the reflector is set up in the way described in Chapter 2. The computer model consists of 310 nodes, 540 membrane elements and 48 cable elements. Three different rib boundaries will be compared: (i) all rib nodes are fully constrained, (ii) all rib nodes (except those at the tip and the root) are allowed to slide in the direction ($\parallel$) to the rib, (iii) all rib nodes (except those at the root) are allowed to slide perpendicular ($\perp$) to the plane of the ribs.

Two different initial prestress distributions are considered. The first distribution is obtained from the first prestressing strategy, for $t_{x1} = 80$ N/m and $t_{x2} = 80$ N/m. The second distribution is obtained from the second prestressing strategy, for $t_{x1} = 80$ N/m and $t_{y1} = 100$ N/m. Figure 4.2 shows the two prestress distributions, for the standard configuration case; the length of each segment is proportional to the stress magnitude.

4.2 Equilibrium Surface

The equilibrium surface achieves the best rms error with an acceptable prestress distribution (Lai, You and Pellegrino 1997). Table 4.3 shows the rms errors of the equilibrium surfaces of reflectors with standard and central hub configurations. Comparing the results in Table 4.2 and Table 4.3, it is clear that the error of the equilibrium surfaces is within 10 and 20% of the reference surface.

The last column in Table 4.3 identifies the figure that shows the shape and prestress distribution, for each of the 12 different reflectors that have been analysed.

The stress in the membrane has to be kept low to avoid problems such as rib buckling, or long-term stretching of the membrane. The stress distributions computed for the standard configuration reflector, Table 4.4, tend to have a

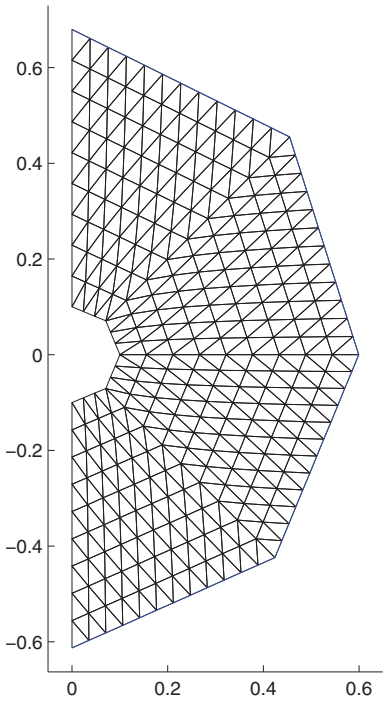

(a) Standard configuration

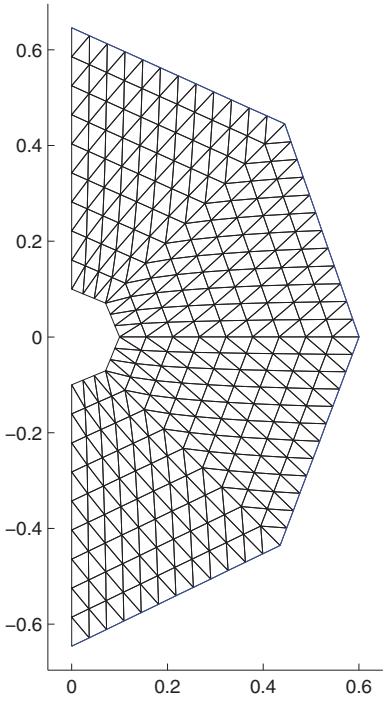

(b) Central hub configuration

Figure 4.1: Plan views of initial meshes of 1.2 m reflectors with different configurations.

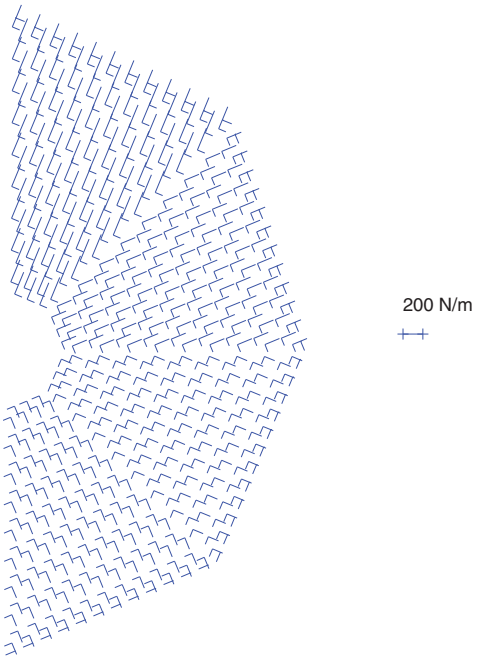

(a) Prestress strategy 1 ($t_{x1} = 80$ N/m and $t_{x2} = 80$ N/m)

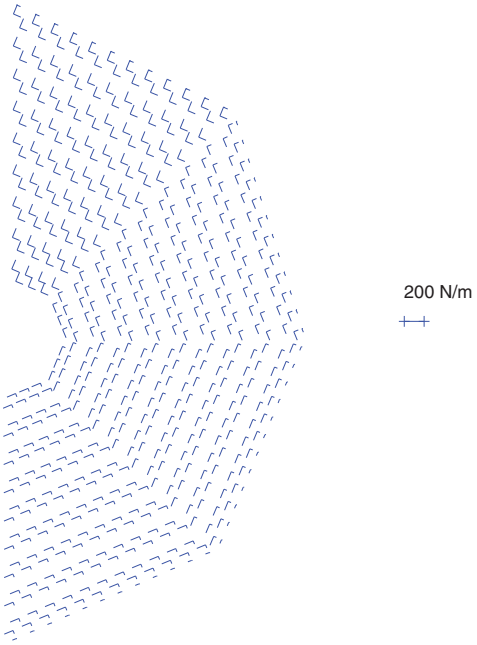

(b) Prestress strategy 2 ($t_{x1} = 80$ N/m and $t_{y1} = 100$ N/m)

Figure 4.2: Direction and magnitude of initial prestress distribution (standard configuration).

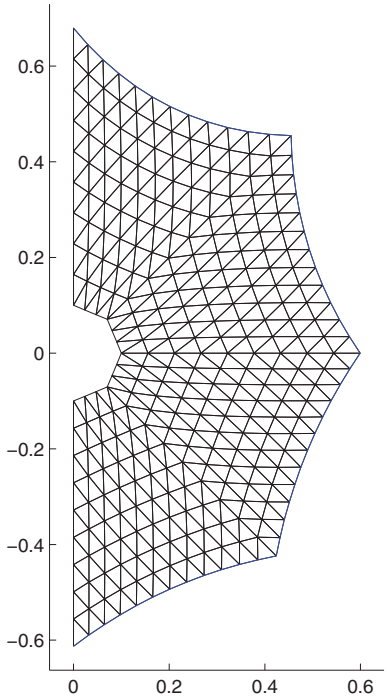

(a) Equilibrium shape after form-finding.

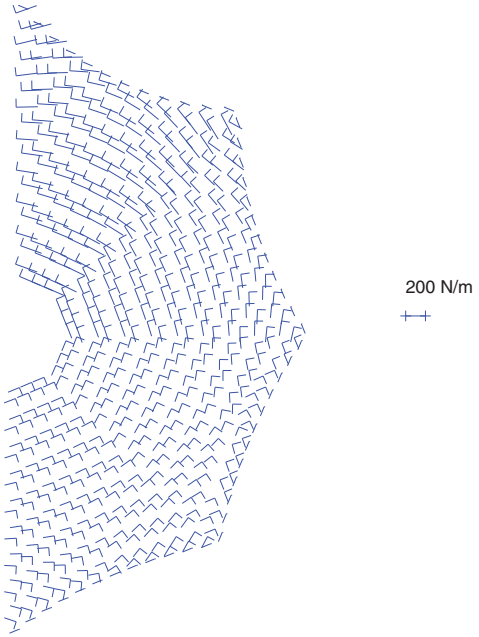

(b) Direction and magnitude of principal stresses.

Figure 4.3: Standard configuration reflector with fixed boundary (prestress strategy 1).

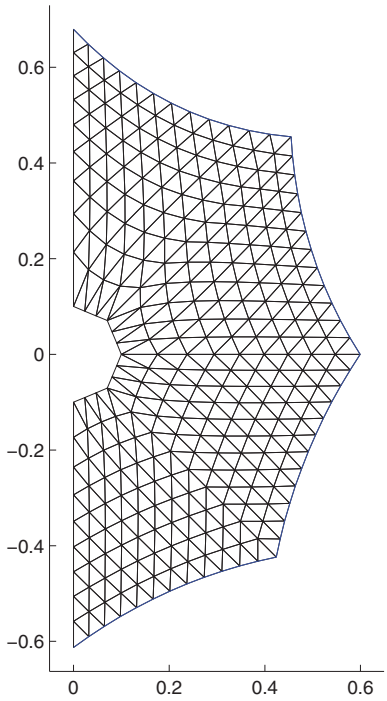

(a) Equilibrium shape after form-finding.

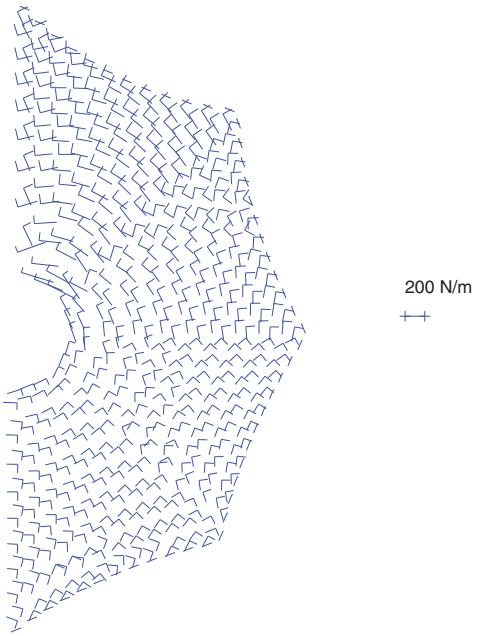

(b) Direction and magnitude of principal stresses.

Figure 4.4: Standard configuration reflector with sliding ‖ boundary (prestress strategy 1).

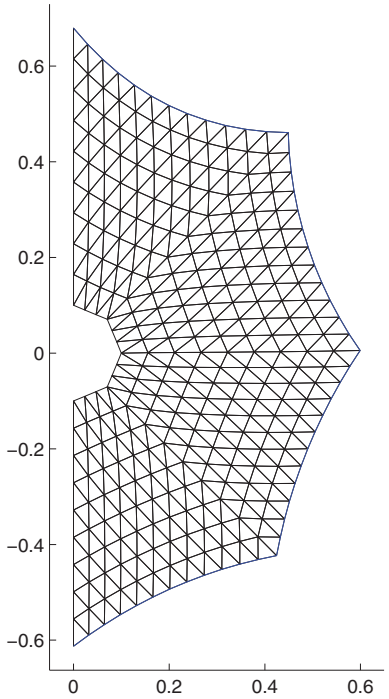

(a) Equilibrium shape after form-finding.

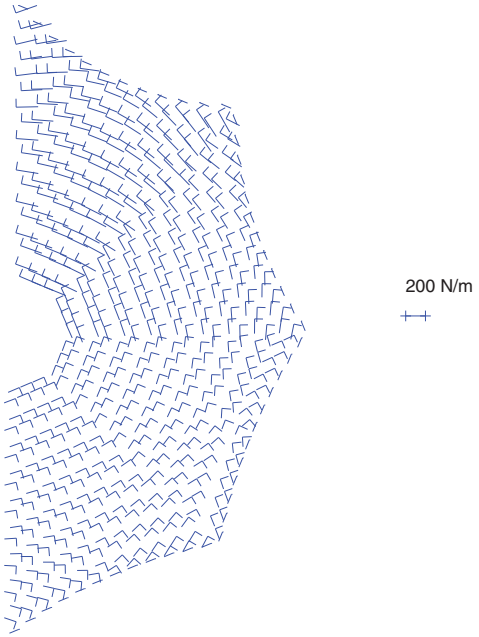

(b) Direction and magnitude of principal stresses.

Figure 4.5: Standard configuration reflector with sliding $\perp$ boundary (prestress strategy 1).

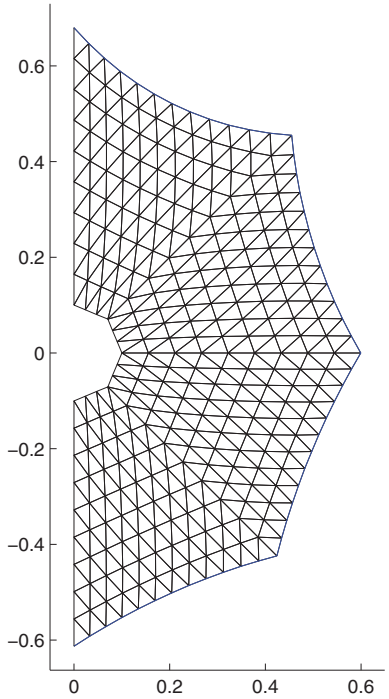

(a) Equilibrium shape after form-finding.

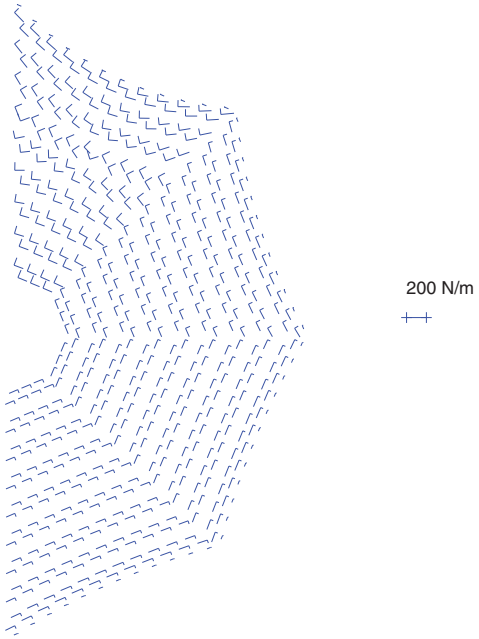

(b) Direction and magnitude of principal stresses.

Figure 4.6: Standard configuration reflector with fixed boundary (prestress strategy 2).

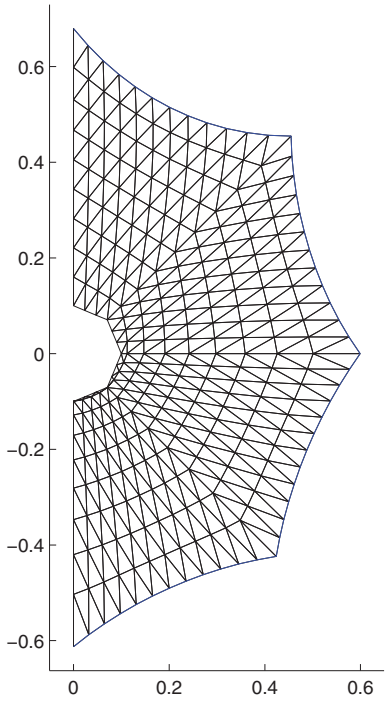

(a) Equilibrium shape after form-finding.

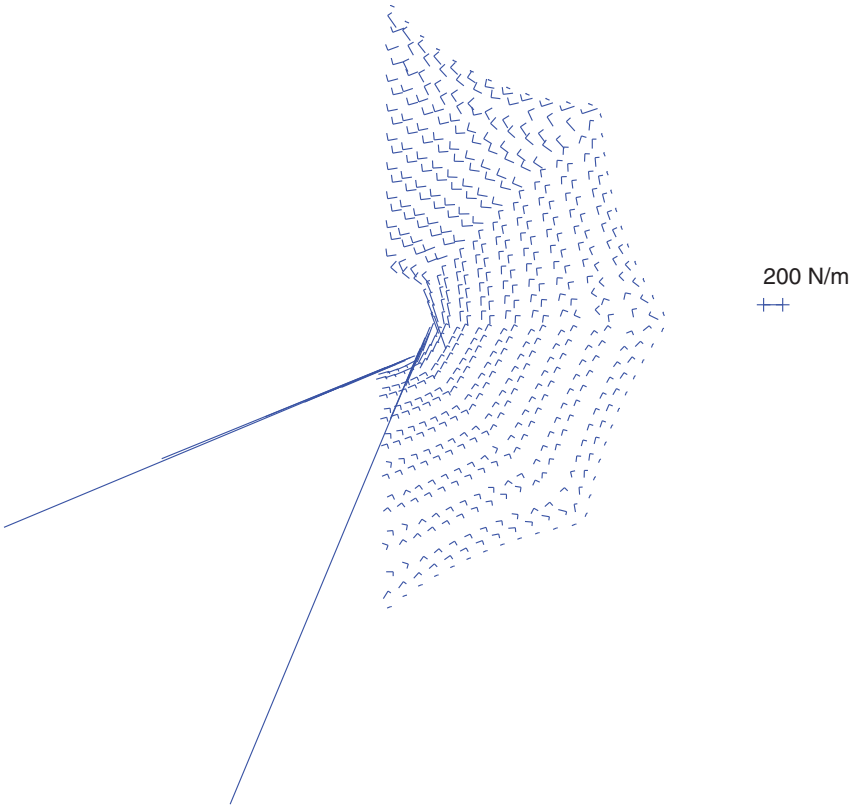

(b) Direction and magnitude of principal stresses.

Figure 4.7: Standard configuration reflector with sliding ‖ boundary (prestress strategy 2).

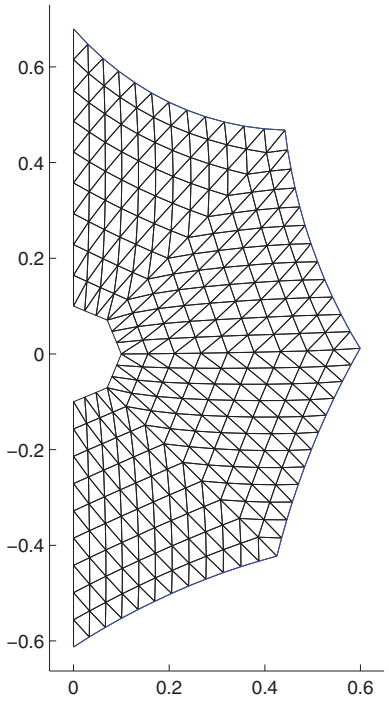

(a) Equilibrium shape after form-finding.

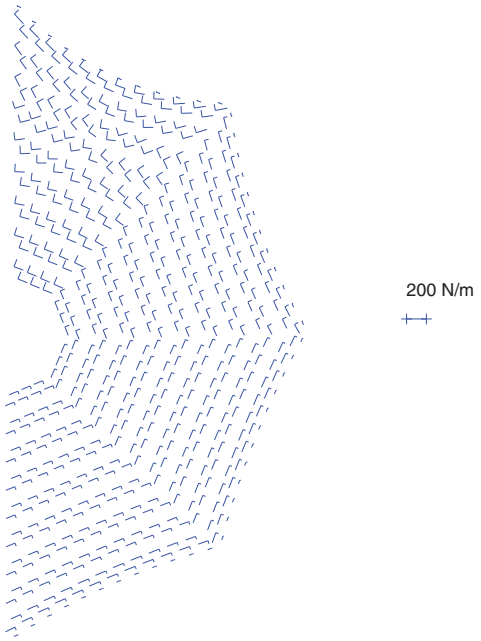

(b) Direction and magnitude of principal stresses.

Figure 4.8: Standard configuration reflector with sliding $\perp$ boundary (prestress strategy 2).

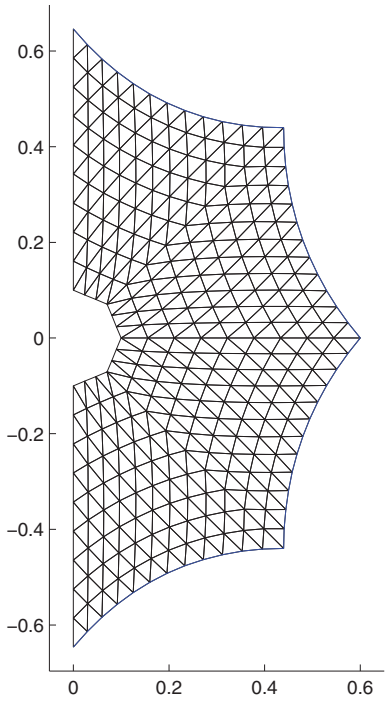

(a) Equilibrium shape after form-finding.

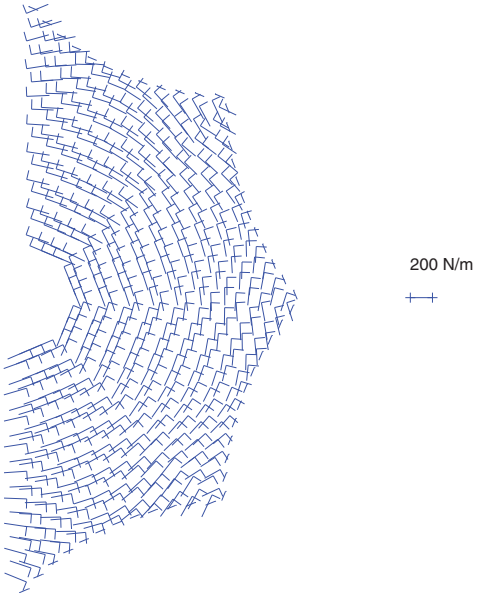

(b) Direction and magnitude of principal stresses.

Figure 4.9: Central hub configuration reflector with fixed boundary (prestress strategy 1).

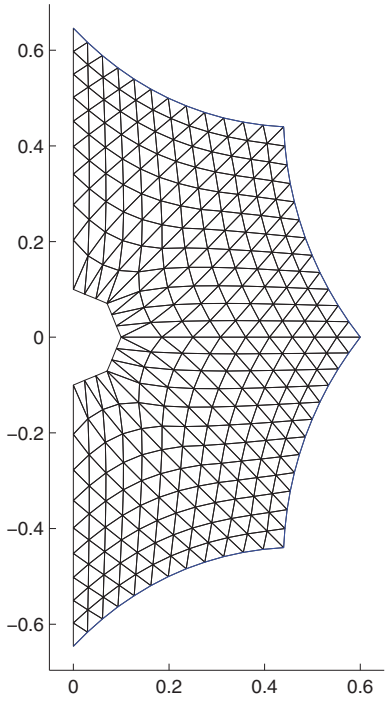

(a) Equilibrium shape after form-finding.

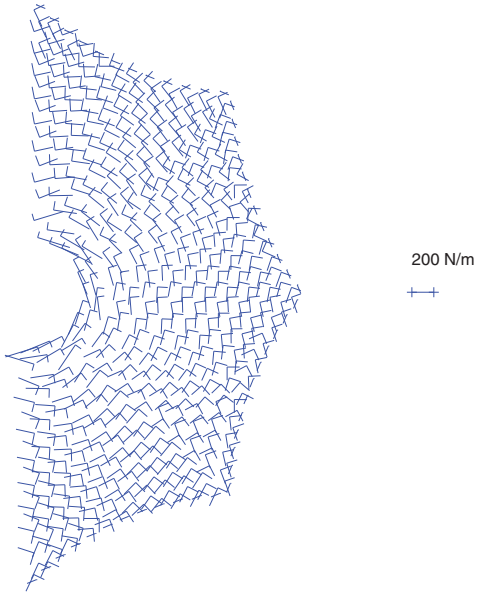

(b) Direction and magnitude of principal stress.

Figure 4.10: Central hub configuration reflector with sliding ‖ boundary (prestress strategy 1).

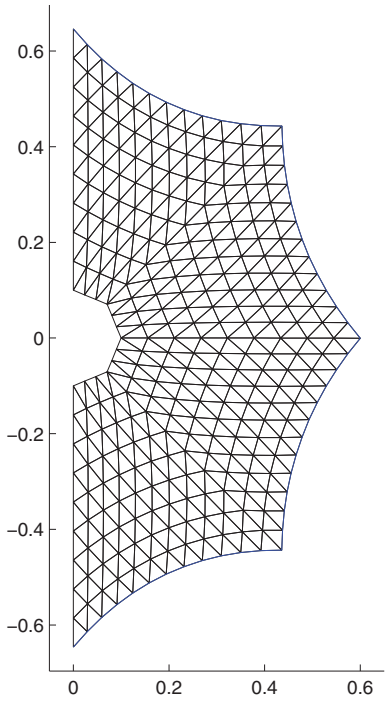

(a) Equilibrium shape after form-finding.

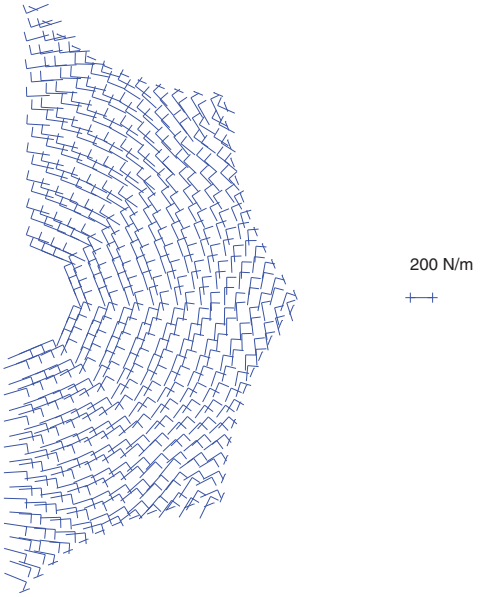

(b) Direction and magnitude of principal stresses.

Figure 4.11: Central hub configuration reflector with sliding $\perp$ boundary (pre-stress strategy 1).

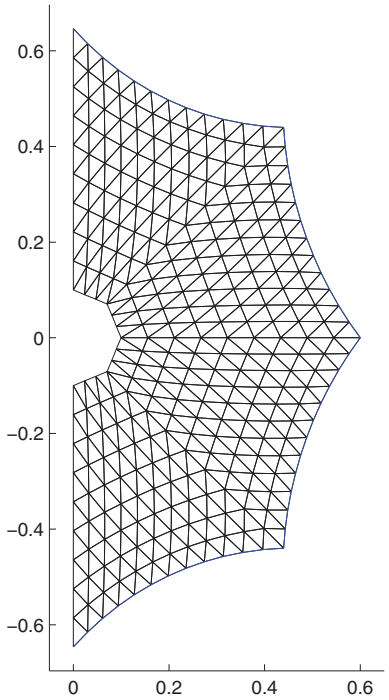

(a) Equilibrium shape after form-finding.

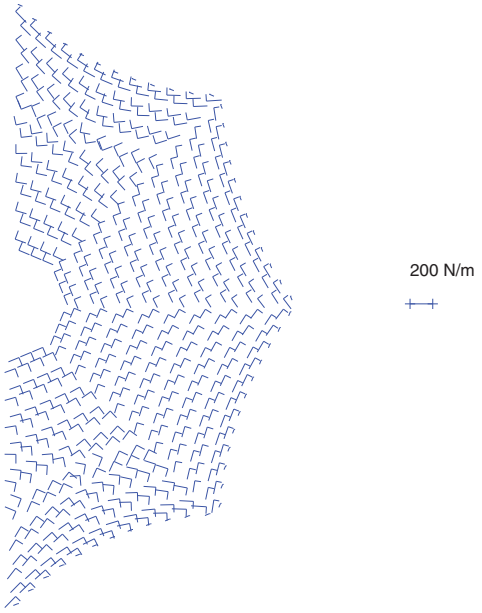

(b) Direction and magnitude of principal stresses.

Figure 4.12: Central hub configuration reflector with fixed boundary (prestress strategy 2).

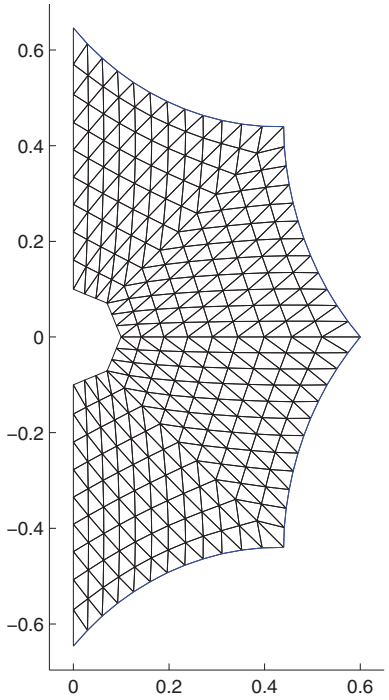

(a) Equilibrium shape after form-finding.

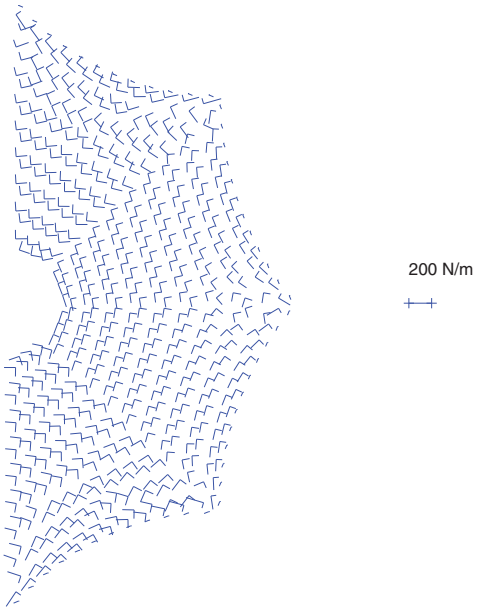

(b) Direction and magnitude of principal stresses.

Figure 4.13: Central hub configuration reflector with sliding || boundary (prestress strategy 2).

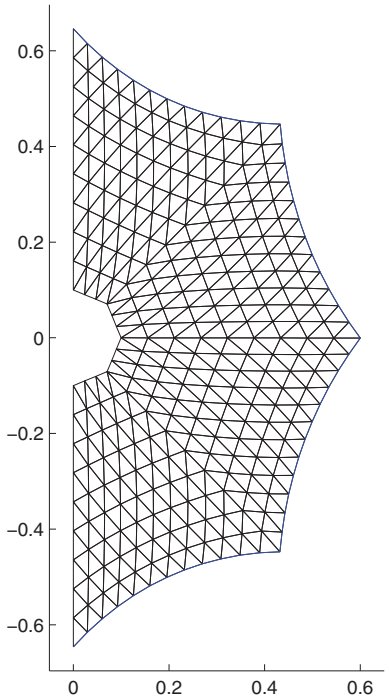

(a) Equilibrium shape after form-finding.

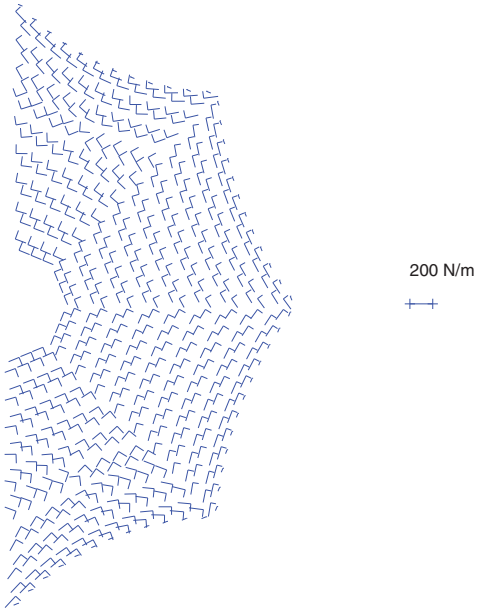

(b) Direction and magnitude of principal stresses.

Figure 4.14: Central hub configuration reflector with sliding $\perp$ boundary (pre-stress strategy 2).

Configuration	Prestress	b.c.	rms error [mm]	Ref.
Standard	Strategy 1	Fixed	4.0	fig. 4.3
		Sliding $\parallel$	3.8	fig. 4.4
		Sliding $\perp$	4.0	fig. 4.5
	Strategy 2	Fixed	3.5	fig. 4.6
		Sliding $\parallel$	3.9	fig. 4.7
		Sliding $\perp$	3.5	fig. 4.8
Central hub	Strategy 1	Fixed	4.1	fig. 4.9
		Sliding $\parallel$	3.9	fig. 4.10
		Sliding $\perp$	4.1	fig. 4.11
	Strategy 2	Fixed	3.7	fig. 4.12
		Sliding $\parallel$	3.7	fig. 4.13
		Sliding $\perp$	3.6	fig. 4.14

Table 4.3: Rms errors of equilibrium surfaces

higher maximum principal stress and a lower minimum principal stress than the distributions computed for the central hub configuration, Table 4.5.

Excluding one particular sets of "anomalous" results in Table 4.4, showing very large maximum stresses, the maximum stress ratio is between about 3 and 6 in Table 4.4, and between about 2.5 and 5 in Table 4.5, which are all acceptable in terms of avoiding wrinkling of the membrane. On the whole, the best stress distributions are those obtained for the central hub configuration using the second prestress strategy, as the maximum stresses are lowest —about 150 N/m— and the minimum stresses are highest —about 40 N/mm—. Note that the effect of changing the boundary conditions is very small in this case.

Prestress strategy	b.c.	Principal stress					
		σ_1 (N/m)		σ_2 (N/m)		ratio (σ_1/σ_2)	
		max	min	max	min	max	min
1	Fixed	239.5	96.7	104.4	78.3	3.00	1.02
	Slide $\parallel$	343.5	96.1	130.2	55.8	6.13	1.01
	Slide $\perp$	241.8	96.7	104.4	77.9	3.06	1.02
2	Fixed	134.8	89.6	89.2	25.7	4.48	1.01
	Slide $\parallel$	5.14×10^3	56.2	88.6	0.57	8.98×10^3	1.01
	Slide $\perp$	134.8	89.6	89.1	25.7	4.48	1.01

Table 4.4: Principal stresses in standard configuration reflector.

Prestress strategy	b.c.	Principal stress					
		σ_1 (N/m)		σ_2 (N/m)		ratio (σ_1/σ_2)	
		max	min	max	min	max	min
1	Fixed	220.2	135.5	105.9	78.8	2.74	1.34
	Slide $\parallel$	308.8	118.9	127.1	57.3	5.39	1.03
	Slide $\perp$	223.2	134.0	104.8	79.3	2.82	1.31
2	Fixed	136.1	86.0	89.3	48.9	2.33	1.00
	Slide $\parallel$	160.97	77.32	88.8	46.7	3.24	1.01
	Slide $\perp$	136.4	86.1	88.9	45.9	2.64	1.01

Table 4.5: Principal stresses in central hub configuration reflector.

4.3 Rib Loads

Figure 4.15 defines the force components on a rib; the in-plane force components at node i are N_{xi} and N_{zi}, and the out-of-plane forces are N_{yi}.

Table 4.6 and Table 4.7 list the Euclidean norms of the intermediate in-plane forces, $\sqrt{\sum_{i=1}^{n-1}(N_{xi}^2 + N_{zi}^2)}$, and of the out-of-plane forces, $\sqrt{\sum_{i=1}^{n-1} N_{yi}^2}$. The tables list also the absolute values of the tip force components, for the twelve different cases that have been considered in Section 4.2.

Note that the intermediate forces are small in comparison with the tip forces. Also note that the tip forces are smallest for the central hub configuration when prestress strategy 2 is used.

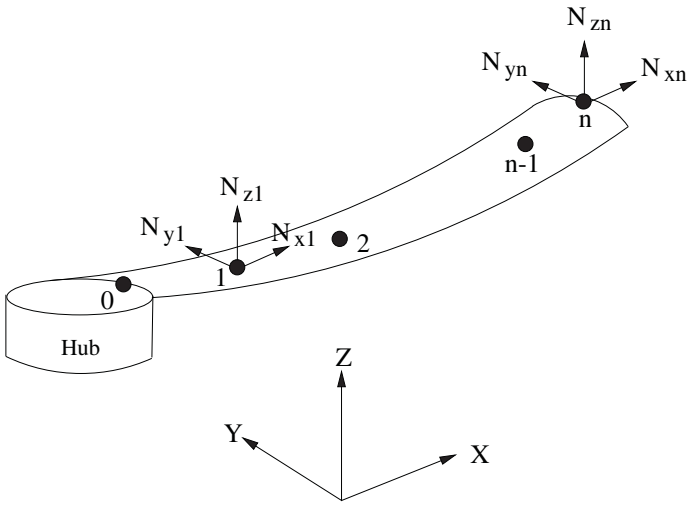

Figure 4.15: Force components on a rib.

Prestress strategy	b.c.	Rib	Intermediate		Tip	
			out-plane	in-plane	out-plane	in-plane
1	Fixed	1	0.00	15.40	0.00	169.74
		2	0.17	9.88	3.79	149.56
		3	0.13	4.76	1.65	118.68
		4	0.03	4.21	0.45	117.32
		5	0.00	4.96	0.00	125.86
	Slide $\parallel$	1	1.00	5.29	0.00	151.24
		2	0.93	4.32	5.52	137.52
		3	0.61	3.38	2.65	114.41
		4	0.15	3.51	0.43	115.14
		5	0.00	3.89	0.00	123.18
	Slide $\perp$	1	0.00	15.76	0.00	167.88
		2	0.00	10.06	0.00	148.87
		3	0.00	4.71	0.00	119.68
		4	0.00	4.19	0.00	118.10
		5	0.00	4.94	0.00	126.12
2	Fixed	1	0.00	4.72	0.00	72.84
		2	0.33	5.46	4.08	59.69
		3	0.09	7.02	1.50	42.61
		4	0.02	7.93	0.38	42.01
		5	0.00	8.28	0.00	45.54
	Slide $\parallel$	1	0.00	3.21	0.00	78.56
		2	2.02	2.70	4.51	67.23
		3	2.16	2.26	1.74	50.47
		4	0.79	2.37	0.09	50.43
		5	0.00	2.57	0.00	54.71
	Slide $\perp$	1	0.00	4.48	0.00	71.16
		2	0.00	5.31	0.00	59.08
		3	0.00	7.16	0.00	43.46
		4	0.00	8.08	0.00	42.68
		5	0.00	8.38	0.00	45.76

Table 4.6: Out-of-plane and in-plane forces (N) acting on the ribs of standard configuration reflector.

Prestress strategy	b.c.	Rib	Intermediate		Tip	
			out-plane	in-plane	out-plane	in-plane
1	Fixed	1	0.00	12.16	0.00	144.73
		2	0.09	9.16	2.35	131.56
		3	0.05	7.06	0.19	117.95
		4	0.12	9.51	2.61	131.48
		5	0.00	12.69	0.00	144.63
	Slide $\parallel$	1	0.00	4.47	0.00	130.76
		2	0.41	3.97	3.19	120.93
		3	0.04	3.75	0.19	110.02
		4	0.37	4.69	3.47	120.86
		5	0.00	5.67	0.00	130.67
	Slide $\perp$	1	0.00	12.33	0.00	143.80
		2	0.00	9.15	0.00	131.59
		3	0.00	6.96	0.00	119.05
		4	0.00	9.51	0.00	131.45
		5	0.00	12.85	0.00	143.62
2	Fixed	1	0.00	4.44	0.00	67.10
		2	0.21	4.64	2.68	57.94
		3	0.00	5.08	0.09	48.83
		4	0.22	4.93	2.82	57.91
		5	0.00	4.99	0.00	67.07
	Slide $\parallel$	1	0.00	2.90	0.00	71.78
		2	0.60	2.62	2.86	63.50
		3	0.00	2.52	0.09	54.66
		4	0.59	3.10	3.01	63.45
		5	0.00	3.67	0.00	71.72
	Slide $\perp$	1	0.00	4.30	0.00	66.24
		2	0.00	4.65	0.00	57.97
		3	0.00	5.28	0.00	49.81
		4	0.00	4.92	0.00	57.88
		5	0.00	4.85	0.00	66.13

Table 4.7: Out-of-plane and in-plane forces (N) acting on the ribs of central hub configuration reflector.

4.4 Conclusions

From the results shown in the previous section, it is clear that the best results are obtained for the central hub configuration reflector using prestress strategy 2. There is little difference between the fixed boundary conditions and the sliding $\perp$ boundary conditions and, since it is best to avoid out-of-plane loads on the flexible ribs, the sliding $\perp$ boundary conditions will be adopted from now on.

Additional results for these two boundary conditions are presented. Figure 4.16 and Fig. 4.17 are colour plots of the principal stress distributions. Figure 4.18 shows the magnitude and direction of the in-plane and out-of-plane forces on the ribs. Figure 4.19 shows contour plots of the error distribution in the two surfaces, with respect to the best-fit paraboloid.

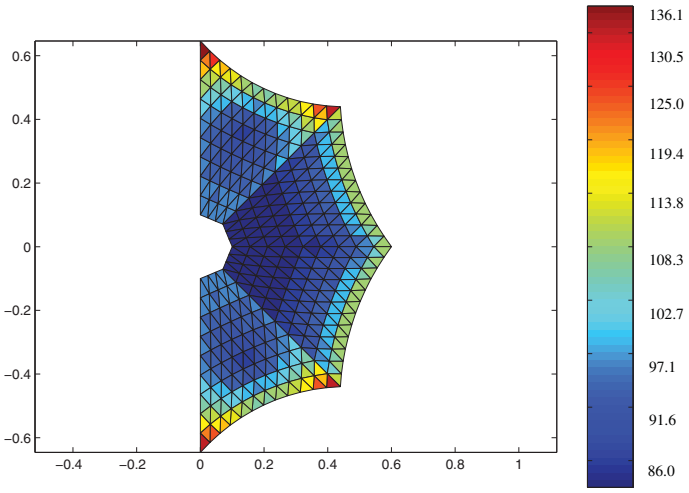

(a) Principal stress $\sigma_1 \times thickness$ (N/m).

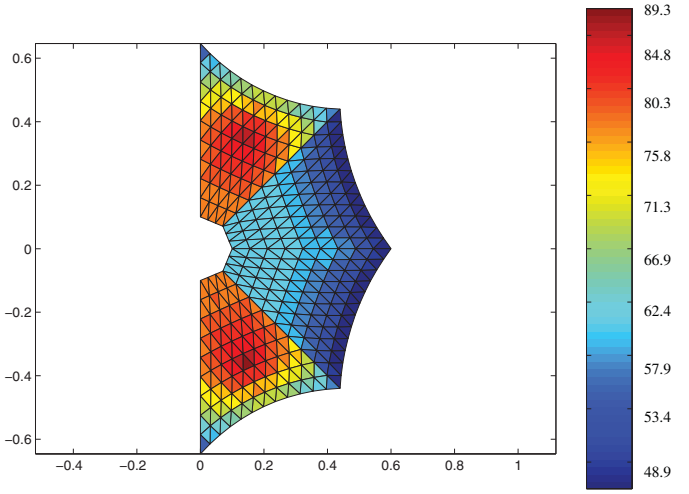

(b) Principal stress $\sigma_2 \times thickness$ (N/m).

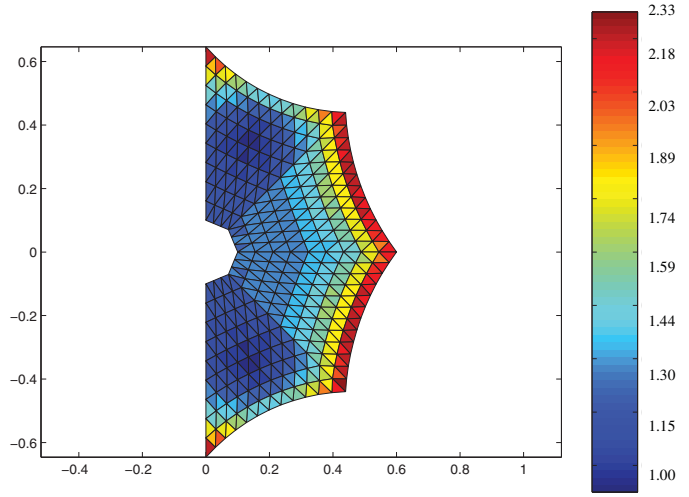

(c) Ratio σ_1/σ_2.

Figure 4.16: Central hub configuration with fixed boundary conditions.

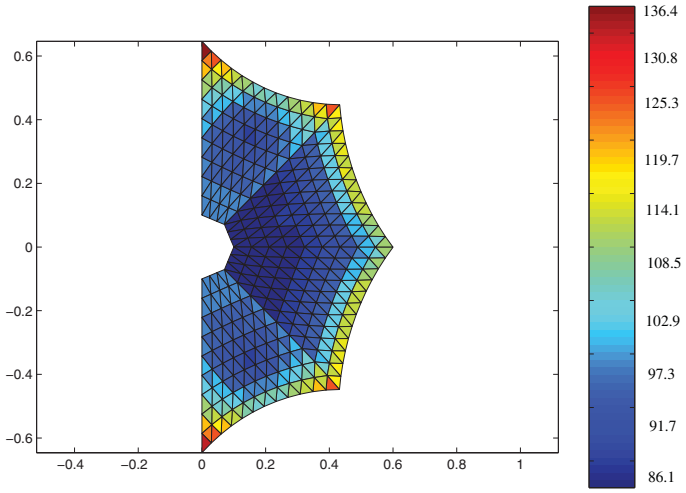

(a) Principal stress $\sigma_1 \times thickness$ (N/m).

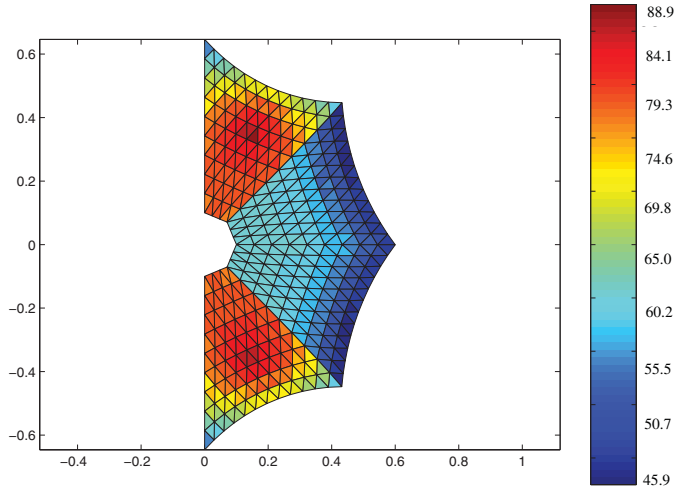

(b) Principal stress $\sigma_2 \times thickness$ (N/m).

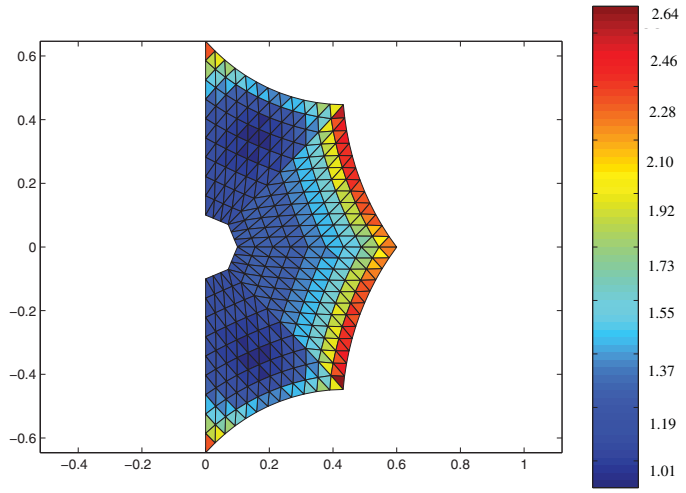

(c) Ratio σ_1/σ_2.

Figure 4.17: Central hub configuration with sliding $\perp$ boundary conditions.

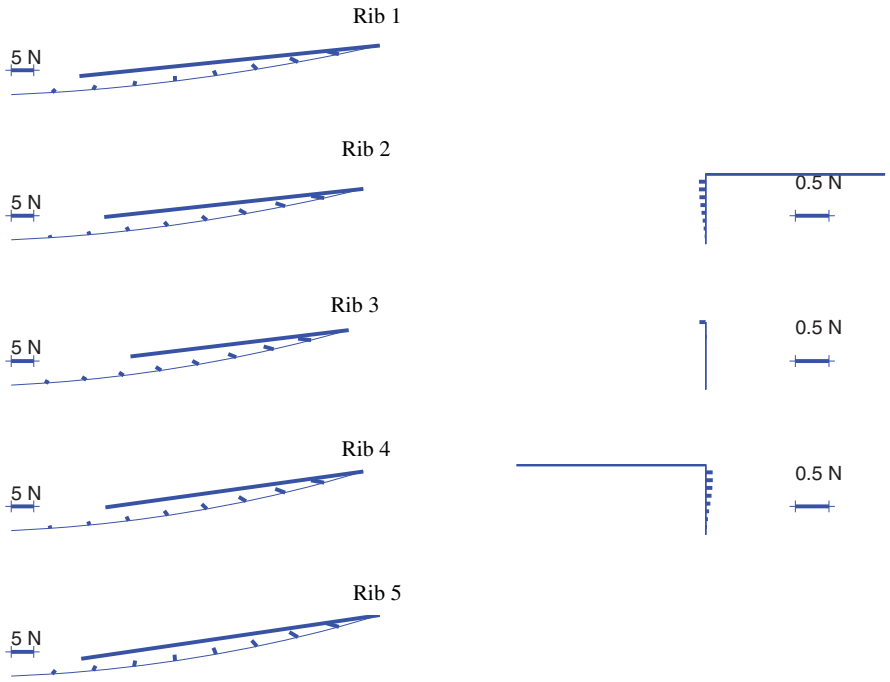

(a) Side view (in-plane), (b) plan view (out-of-plane).
Fixed boundaries

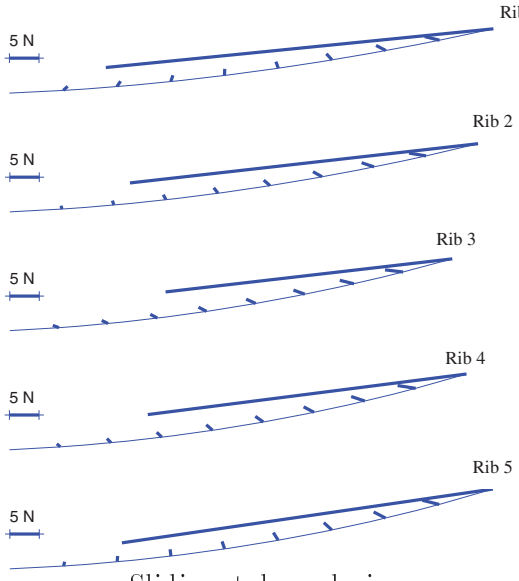

Sliding ⊥ boundaries.

Figure 4.18: Force components along the ribs.

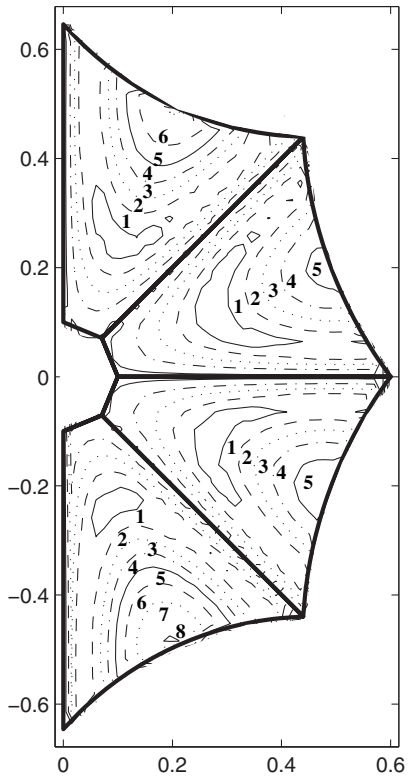

(a) Fixed boundaries

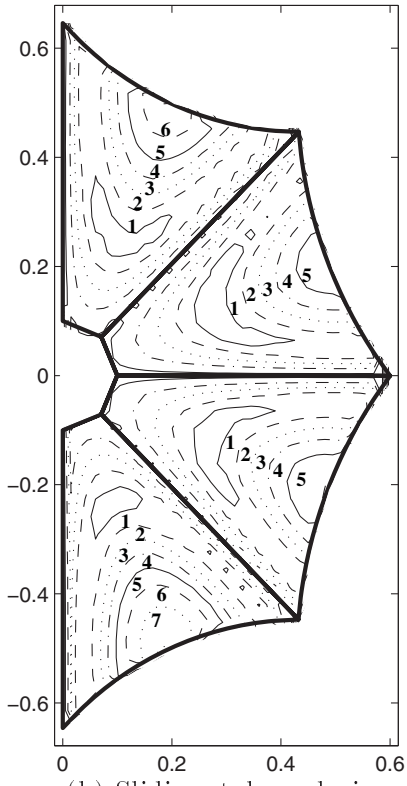

(b) Sliding ⊥ boundaries.

Figure 4.19: Contour plots of error distribution w.r.t. best fit paraboloid (mm).

Chapter 5

Analysis of 1, 3, 5, 10 m Reflectors

This chapter presents our estimates of the stress distribution and rms errors that are achievable in offset CRTS reflectors with the properties given in Table 5.1. These reflectors have the same overall size and number of ribs as the symmetric reflectors analysed in our previous report (Lai, You and Pellegrino 1997).

Since it was shown in the previous chapter that the best combinations of shape and stress distribution are achieved for the central hub configuration whose initial prestress is based on strategy 2, this is the only approach that will be used. Both fixed boundary conditions and sliding $\perp$ boundary conditions will be used.

Diameter (D)	1, 3, 5, 10 m
F/D	0.78
Offset (A)	D/10
Hub diameter	0.2 m
Number of ribs	6, 12, 24, 36 (D= 10 m only)
Configuration	Central hub
Initial prestress	Strategy 2 t_{x1}=80 N/m, t_{y1}=100 N/m

Table 5.1: Properties of offset reflectors that are analysed.

In each analysis we consider half of the reflector, and the total number of nodes and elements used in the model are listed in Table 5.2. These numbers do not change with the diameter of the reflector. The accuracy of the computation is limited by the number of triangular elements used to represent the membrane, but it would not be practical to increase the number of nodes and elements, as the computational time would become unaffordable.

Key results from the analysis are summarised in Table 5.16.

Configuration	no. of nodes	no. of elements
6 ribs	235	405
12 ribs	320	546
24 ribs	402	660
36 ribs	455	720

Table 5.2: Number of nodes and elements used.

5.1 Initial Prestress Strategy

One problem that is encountered when the technique for estimating initial prestress and cord tensions that was developed in Chapter 3 is applied to offset reflectors with many ribs is that the prestress in the gores close to the Y_L axis is almost only in the "hoop" direction, Fig. 5.1(a). Hence, the final stress ratio σ_1/σ_2 becomes very high in these areas (up to 7×10^3), see Fig. 5.1(b). It is likely that this would lead to the formation of wrinkles in the radial direction.

We have found two ways of resolving this difficulty. The first is to change the shape of the membrane so that its projection in the X_L, Y_L plane is a circle, instead of an ellipse. This method is described in Chapter 6. The second way of resolving this difficulty is to consider only 12 ribs when the initial prestress is calculated, see Fig 5.1(c, d). The state of prestress that is calculated in this way is, of course, in equilibrium and has a smaller initial stress ratio that the solution obtained if all 24 ribs are considered. It means that the same prestress will be applied to pairs of adjacent gores, and the cord tensions are calculated by the same method described previously. The disadvantage of this approach is that it does not make the best possible use of all the ribs, as most of the load will fall on the 12 ribs that separate the gores across which we have allowed a stress discontinuity.

Comparing Fig. 5.1(b) and Fig. 5.1(d) it is clear that this method achieves a better stress ratio. However, the out-of-plane rib loading will tend to increase for ribs 3, 5, 7, 9 and 11. The first and last ribs (1 and 13) tend not to be affected because there is little out-of-plane loading near the symmetry plane.

Table 5.3 shows the rib loading that is required by the equilibrium surface (i.e. after form-finding has been carried out) of a 1 m diameter reflector with 24 ribs and fixed boundary conditions. Two initial prestress distributions have been considered, one based on 24 ribs and one on 12 ribs. The table shows that the out-of-plane loading is the most affected; the in-plane loading is also affected, but not as much. Note that the rms error does not change much, from 4.01×10^{-4} mm (24 rib prestressing) to 4.64×10^{-4} mm (12 ribs prestressing).

Tables 5.4-5.6 show the initial prestress distributions of reflectors with 6, 12 and 24 ribs respectively. Because the cord tensions are directly proportional to the diameter of the reflector, see Equation 3.11, and the sag will also increase proportionally with D, the value T/D that is given for each gore in the tables can be used to calculate the actual cord tensions.

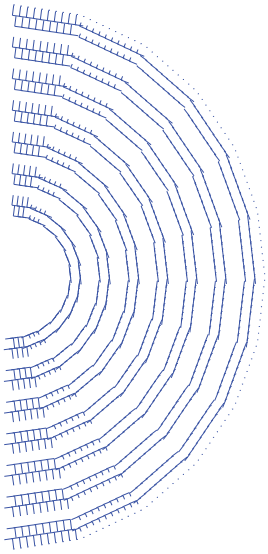

(a) Initial prestress

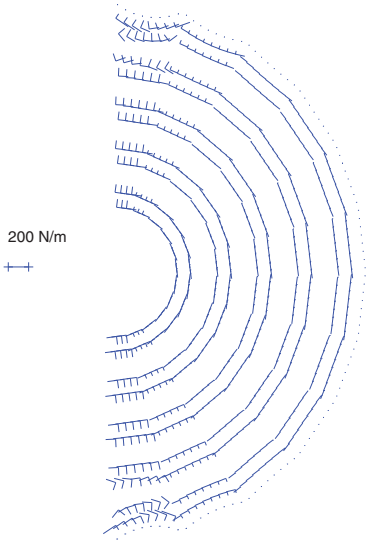

(b) Principal stresses at equilibrium

Prestressing based on 24 ribs

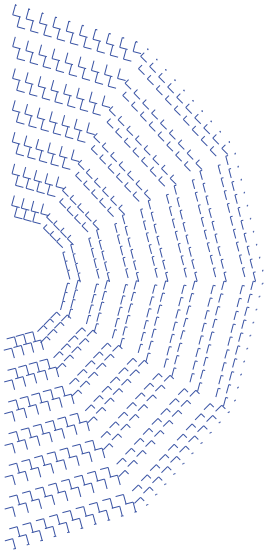

(c) Initial prestress

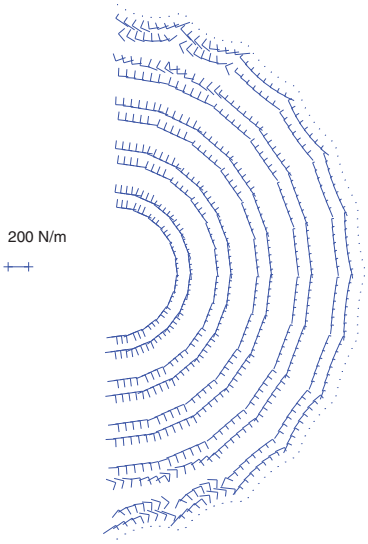

(d) Principal stresses at equilibrium

Prestressing based on 12 ribs

Figure 5.1: Initial and final stress distribution (fixed boundary conditions).

Initial prestress	Rib	Intermediate		Tip	
		out-plane	in-plane	out-plane	in-plane
24 ribs	1	0.00	1.81	0.00	13.55
	2	0.05	1.95	2.16	10.07
	3	0.03	3.23	2.16	4.32
	4	0.03	3.63	0.93	1.66
	5	0.02	3.58	0.18	1.11
	6	0.01	3.49	0.02	1.01
	7	0.02	3.46	0.01	1.00
	8	0.03	3.50	0.04	1.02
	9	0.04	3.59	0.20	1.11
	10	0.04	3.65	0.94	1.66
	11	0.03	3.28	2.17	4.33
	12	0.05	2.12	2.17	10.09
	13	0.00	2.09	0.00	13.58
12 ribs	1	0.00	1.81	0.00	13.55
	2	0.05	1.79	0.39	13.49
	3	0.55	1.93	1.69	10.66
	4	0.23	2.05	0.39	7.68
	5	0.38	2.53	1.13	5.99
	6	0.16	2.68	0.10	4.33
	7	0.01	2.64	0.02	4.30
	8	0.17	2.68	0.13	4.34
	9	0.37	2.57	1.17	6.00
	10	0.24	2.13	0.43	7.69
	11	0.55	2.10	1.72	10.68
	12	0.06	2.06	0.40	13.51
	13	0.00	2.09	0.00	13.58

Table 5.3: Rib loading of 1 m reflector with 24 ribs with fixed boundaries, for initial prestress based on 24 ribs and 12 ribs [N].

	Gore		
	1	2	3
t_x	80.00	84.08	80.00
t_y	100.00	84.69	100.00
T/D	53.85	52.83	53.85

Table 5.4: Initial prestress distribution for 6 rib reflectors [N/m].

	Gore					
	1	2	3	4	5	6
t_x	80.00	84.58	88.68	88.68	84.58	80.00
t_y	100.00	49.85	23.16	23.16	49.85	100.00
T/D	16.84	13.88	12.15	12.15	13.88	16.84

Table 5.5: Initial prestress distribution for 12 rib reflectors [N/m].

	Gore											
	1	2	3	4	5	6	7	8	9	10	11	12
t_x	80.00		84.58		88.68		88.68		84.58		80.00	
t_y	100.00		49.85		23.16		23.16		49.85		100.00	
T/D	6.32	6.36	4.71	4.82	3.68	3.72	3.72	3.68	4.82	4.71	6.36	6.32

Table 5.6: Initial prestress distribution for 24 rib reflectors [N/m].

5.2 1 m Reflector

The rms error of the reference surface and the equilibrium surface of 1 m offset reflectors are listed in Table 5.7. Table 5.8 lists the in-plane and out-of-plane rib loads applied by the equilibrium surface. Figures 5.2, 5.3 show the equilibrium shapes and the principal stress distributions in reflectors with different numbers of ribs, and with fixed and sliding $\perp$ boundary conditions, respectively.

Configuration	Reference surface	Boundary condition	Equilibrium surface
6 ribs	4.8	Fixed	5.1
		Slide $\perp$	5.1
12 ribs	1.3	Fixed	1.6
		Slide $\perp$	1.6
24 ribs	0.3	Fixed	0.5
		Slide $\perp$	0.5

Table 5.7: Rms errors of 1 m diameter reflectors [mm].

Configuration	b.c.	Rib	Intermediate		Tip	
			out-plane	in-plane	out-plane	in-plane
6 ribs	Fixed	1	0.00	4.10	0.00	91.19
		2	0.09	4.07	1.13	83.48
		3	0.12	4.35	1.39	83.44
		4	0.00	4.80	0.00	91.13
	Slide $\perp$	1	0.00	4.06	0.00	90.84
		2	0.00	4.10	0.00	83.73
		3	0.00	4.37	0.00	83.63
		4	0.00	4.74	0.00	90.66
12 ribs	Fixed	1	0.00	3.42	0.00	29.82
		2	0.15	3.56	2.60	24.09
		3	0.07	4.39	1.64	14.96
		4	0.02	4.68	0.03	11.62
		5	0.05	4.46	1.72	14.96
		6	0.16	3.79	2.66	24.09
		7	0.00	3.80	0.00	29.83
	Slide $\perp$	1	0.00	3.18	0.00	28.91
		2	0.00	3.41	0.00	23.71
		3	0.00	4.58	0.00	15.43
		4	0.00	4.96	0.00	12.44
		5	0.00	4.62	0.00	15.41
		6	0.00	3.62	0.00	23.67
		7	0.00	3.56	0.00	28.88
24 ribs	Fixed	1	0.00	1.81	0.00	13.55
		2	0.06	1.79	0.39	13.49
		3	0.55	1.93	1.69	10.66
		4	0.23	2.05	0.39	7.68
		5	0.38	2.53	1.13	5.99
		6	0.16	2.68	0.10	4.33
		7	0.01	2.64	0.02	4.30
		8	0.17	2.69	0.13	4.34
		9	0.37	2.57	1.17	6.00
		10	0.24	2.13	0.43	7.69
		11	0.55	2.10	1.72	10.68
		12	0.06	2.06	0.40	13.51
		13	0.00	2.09	0.00	13.58
	Slide $\perp$	1	0.00	1.71	0.00	13.28
		2	0.00	1.69	0.00	13.21
		3	0.00	1.84	0.00	10.56
		4	0.00	2.05	0.00	7.69
		5	0.00	2.62	0.00	6.14
		6	0.00	2.78	0.00	4.59
		7	0.00	2.80	0.00	4.55
		8	0.00	2.79	0.00	4.59
		9	0.00	2.65	0.00	6.13
		10	0.00	2.12	0.00	7.69
		11	0.00	1.99	0.00	10.57
		12	0.00	1.96	0.00	13.21
		13	0.00	2.09	0.00	13.29

Table 5.8: Rib loads for 1 m diameter reflectors [N].

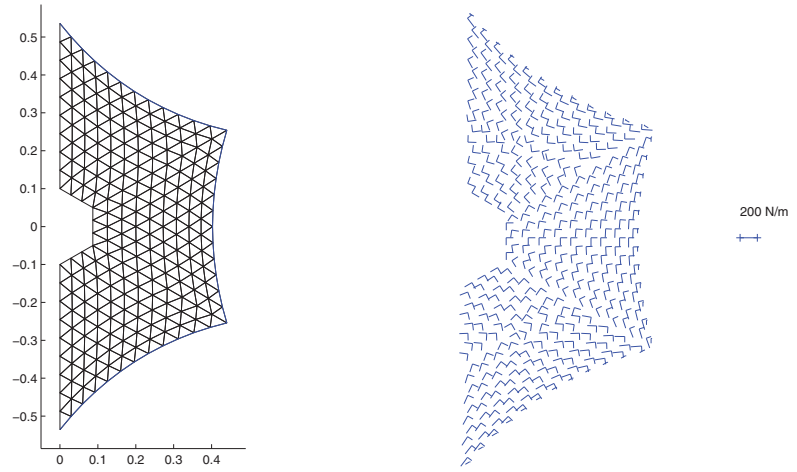

(a) 6 rib configuration

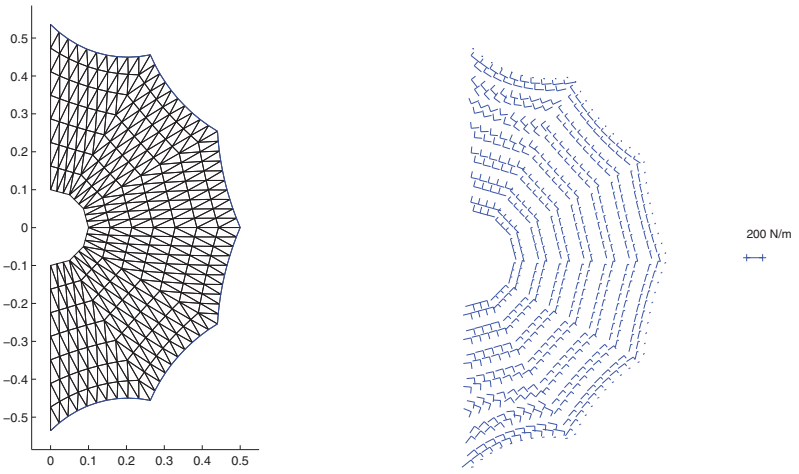

(b) 12 rib configuration

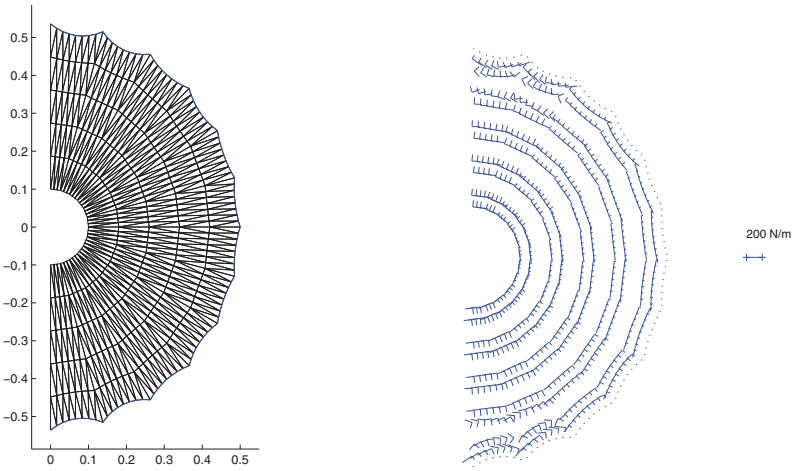

(c) 24 rib configuration

Figure 5.2: Shape and stress distributions of equilibrium shape of 1 m reflector with fixed boundary conditions.

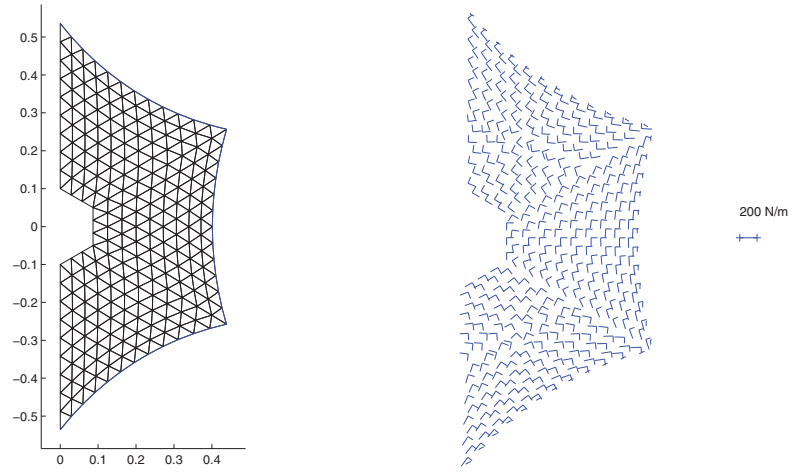

(a) 6 rib configuration

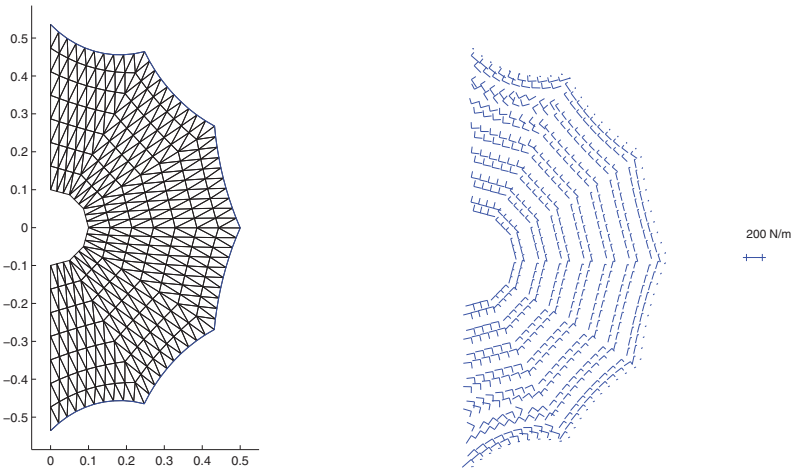

(b) 12 rib configuration

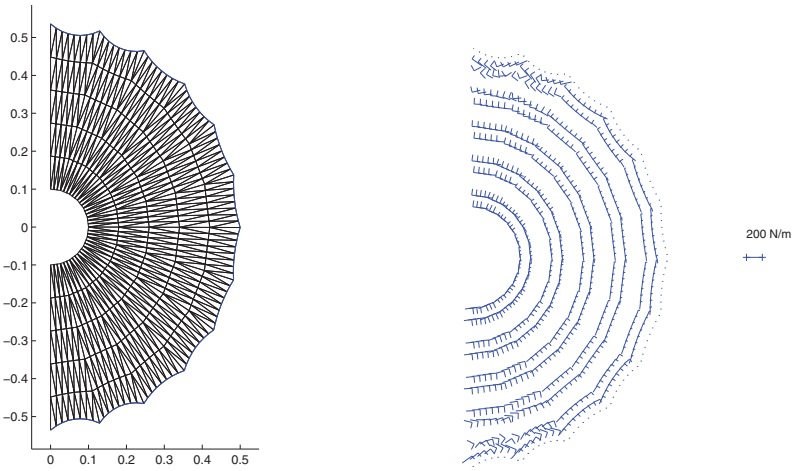

(c) 24 rib configuration

Figure 5.3: Shape and stress distributions of equilibrium shape of 1 m reflector with sliding $\perp$ boundary conditions.

5.3 3 m Reflector

The rms error of reference surface and equilibrium surface of 3 m offset reflectors are listed in Table 5.9. Table 5.10 lists the in-plane and out-of-plane rib loads applied by the equilibrium surface. Figures 5.4, 5.5 show the equilibrium shapes and the principal stress distributions in reflectors with different numbers of ribs, and with fixed and sliding $\perp$ boundary conditions, respectively.

Configuration	Reference surface	Boundary condition	Equilibrium surface
6 ribs	14.7	Fixed	15.4
		Slide $\perp$	15.4
12 ribs	4.0	Fixed	4.9
		Slide $\perp$	4.9
24 ribs	1.1	Fixed	1.5
		Slide $\perp$	1.5

Table 5.9: Rms errors of 3 m diameter offset reflectors [mm].

Confi-guration	b.c.	Rib	Intermediate		Tip	
			out-plane	in-plane	out-plane	in-plane
6 ribs	Fixed	1	0.00	13.57	0.00	274.00
		2	0.30	13.27	3.39	250.97
		3	0.41	14.19	4.19	250.86
		4	0.00	15.79	0.00	273.83
	Slide $\perp$	1	0.00	13.45	0.00	272.93
		2	0.00	13.36	0.00	251.73
		3	0.00	14.26	0.00	251.43
		4	0.00	15.64	0.00	272.40
12 ribs	Fixed	1	0.00	10.79	0.00	90.22
		2	0.48	11.20	7.75	73.06
		3	0.25	14.77	4.88	45.58
		4	0.06	15.83	0.11	35.49
		5	0.19	14.96	5.11	45.58
		6	0.49	11.96	7.50	73.08
		7	0.00	12.03	0.00	90.26
	Slide $\perp$	1	0.00	10.13	0.00	87.46
		2	0.00	10.74	0.00	71.89
		3	0.00	15.33	0.00	47.02
		4	0.00	16.66	0.00	38.02
		5	0.00	15.47	0.00	46.95
		6	0.00	11.44	0.00	71.79
		7	0.00	11.34	0.00	87.36
24 ribs	Fixed	1	0.00	5.49	0.00	41.25
		2	0.19	5.44	1.18	41.05
		3	1.88	6.02	5.01	32.56
		4	0.75	6.69	1.21	23.50
		5	1.32	8.61	3.33	18.43
		6	0.52	9.10	0.30	13.40
		7	0.03	8.97	0.06	13.30
		8	0.57	9.13	0.40	13.40
		9	1.30	8.74	3.44	18.45
		10	0.77	6.94	1.32	23.52
		11	1.90	6.56	5.10	32.62
		12	0.19	6.34	1.23	41.11
		13	0.00	6.44	0.00	41.31
	Slide $\perp$	1	0.00	5.20	0.00	40.39
		2	0.00	5.14	0.00	40.16
		3	0.00	5.78	0.00	32.25
		4	0.00	6.70	0.00	23.55
		5	0.00	8.84	0.00	18.89
		6	0.00	9.31	0.00	14.21
		7	0.00	9.35	0.00	14.08
		8	0.00	9.33	0.00	14.20
		9	0.00	8.92	0.00	18.89
		10	0.00	6.90	0.00	23.53
		11	0.00	6.28	0.00	32.26
		12	0.00	6.05	0.00	40.17
		13	0.00	6.15	0.00	40.40

Table 5.10: Rib loads for 3 m diameter reflector [N].

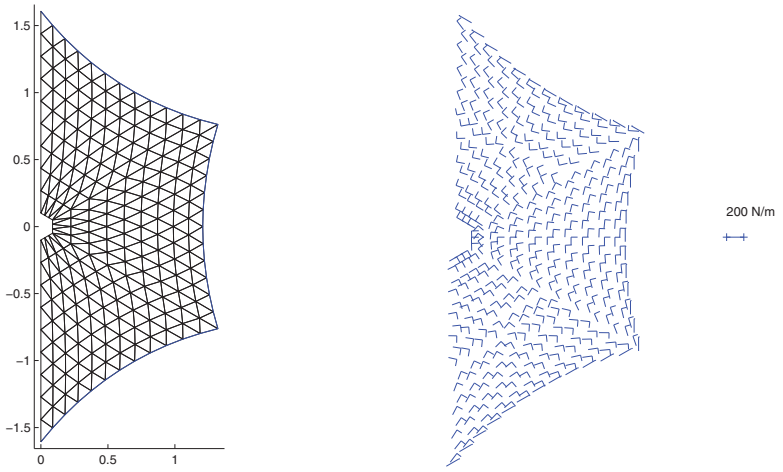

(a) 6 rib configuration

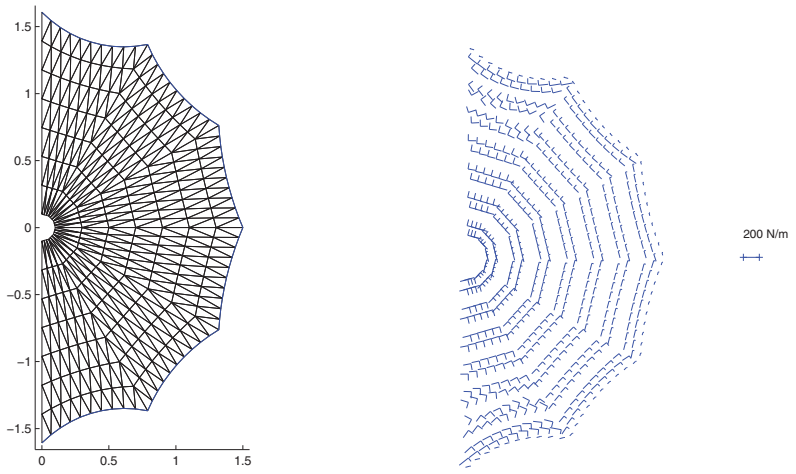

(b) 12 rib configuration

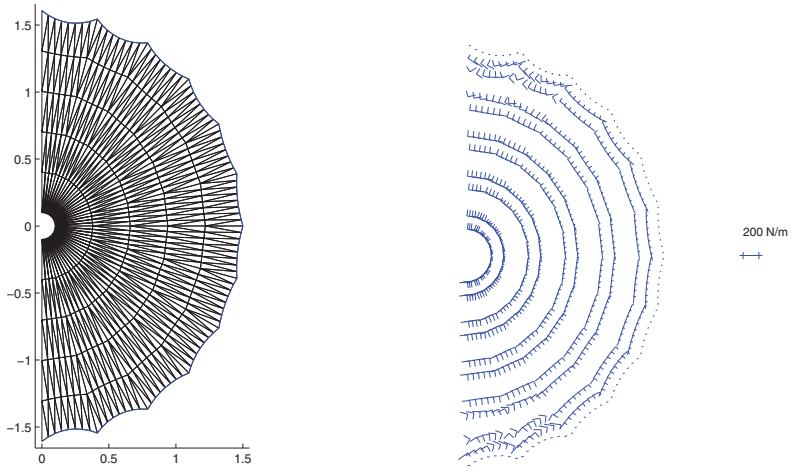

(c) 24 rib configuration

Figure 5.4: Shape and stress distributions of equilibrium shape of 3 m reflector with fixed boundary conditions.

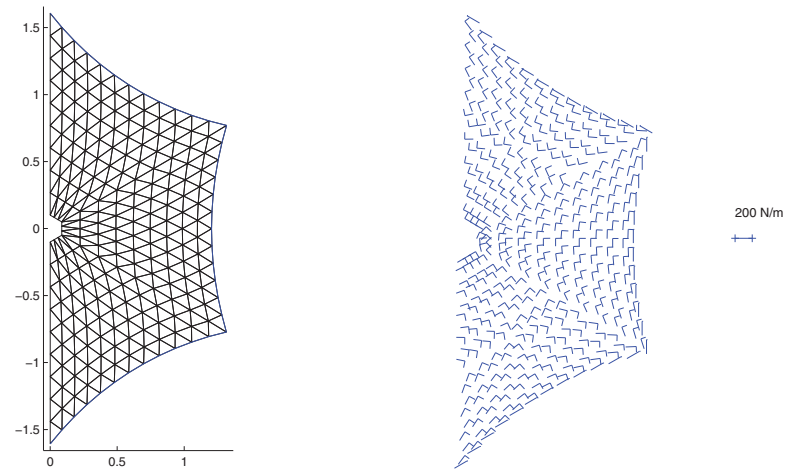

(a) 6 rib configuration

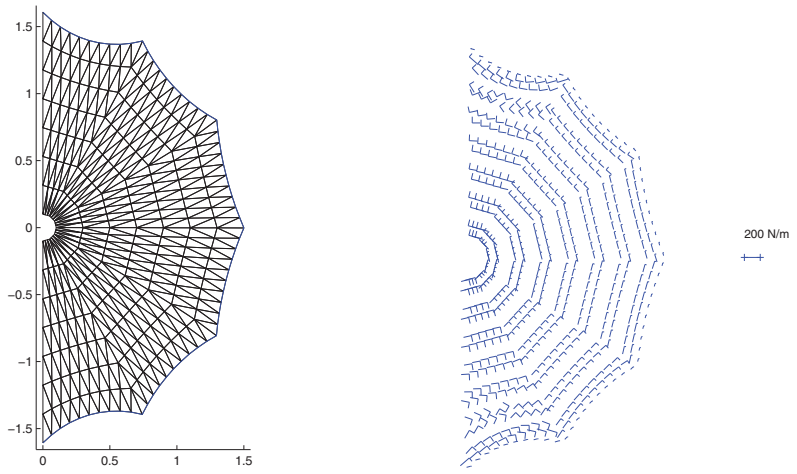

(b) 12 rib configuration

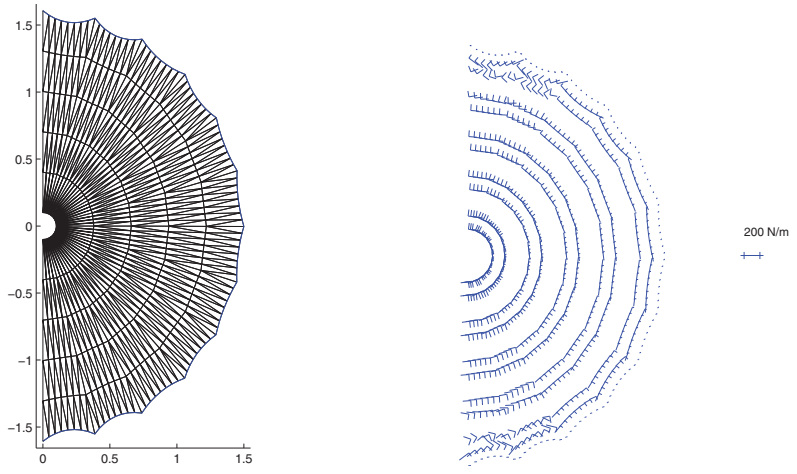

(c) 24 rib configuration

Figure 5.5: Shape and stress distribution of equilibrium shape of 3 m reflector with sliding $\perp$ boundary conditions.

5.4 5 m Reflector

The rms error of the reference surface and the equilibrium surface of 5 m offset reflectors are listed in Table 5.11. Table 5.12 lists the in-plane and out-of-plane rib loads applied by the equilibrium surface. Figures 5.6, 5.7 show the equilibrium shapes and the principal stress distributions in reflectors with different numbers of ribs, and with fixed and sliding $\perp$ boundary conditions, respectively.

Configuration	Reference surface	Boundary condition	Equilibrium surface
6 ribs	24.6	Fixed	25.7
		Slide $\perp$	25.7
12 ribs	6.7	Fixed	8.2
		Slide $\perp$	8.1
24 ribs	1.8	Fixed	2.5
		Slide $\perp$	2.6

Table 5.11: Rms errors of 5 m diameter offset reflectors [mm].

Configuration	b.c.	Rib	Intermediate		Tip	
			out-plane	in-plane	out-plane	in-plane
6 ribs	Fixed	1	0.00	23.01	0.00	456.81
		2	0.51	22.40	5.65	418.45
		3	0.69	23.96	6.98	418.27
		4	0.00	26.75	0.00	456.54
	Slide $\perp$	1	0.00	22.82	0.00	455.02
		2	0.00	22.57	0.00	419.73
		3	0.00	24.08	0.00	419.23
		4	0.00	26.49	0.00	454.14
12 ribs	Fixed	1	0.00	18.16	0.00	150.61
		2	0.81	18.83	12.90	122.01
		3	0.43	25.14	8.12	76.19
		4	0.09	26.93	0.18	59.35
		5	0.33	25.47	8.50	76.19
		6	0.83	20.12	13.23	122.06
		7	0.00	20.75	0.00	150.68
	Slide $\perp$	1	0.00	17.06	0.00	145.99
		2	0.00	18.05	0.00	120.06
		3	0.00	26.08	0.00	78.61
		4	0.00	28.32	0.00	63.58
		5	0.00	26.31	0.00	78.49
		6	0.00	19.24	0.00	119.90
		7	0.00	19.11	0.00	145.83
24 ribs	Fixed	1	0.00	9.20	0.00	68.93
		2	0.32	9.11	1.97	68.59
		3	3.21	10.13	8.32	54.45
		4	1.28	11.33	2.02	39.31
		5	2.26	14.71	5.52	30.85
		6	0.89	15.50	0.50	22.46
		7	0.05	15.27	0.09	22.29
		8	0.97	15.56	0.68	22.46
		9	2.22	14.92	5.71	30.89
		10	1.31	11.75	2.21	39.34
		11	3.23	11.05	8.48	54.54
		12	0.33	10.63	2.06	68.68
		13	0.00	10.80	0.00	69.02
	Slide $\perp$	1	0.00	8.70	0.00	67.48
		2	0.00	8.60	0.00	67.09
		3	0.00	9.74	0.00	53.92
		4	0.00	11.34	0.00	39.40
		5	0.00	15.07	0.00	31.63
		6	0.00	15.82	0.00	23.83
		7	0.00	15.88	0.00	23.60
		8	0.00	15.85	0.00	23.81
		9	0.00	15.21	0.00	31.63
		10	0.00	11.68	0.00	39.35
		11	0.00	10.58	0.00	53.94
		12	0.00	10.14	0.00	67.10
		13	0.00	10.31	0.00	67.49

Table 5.12: Rib loads for 5 m diameter reflectors [N].

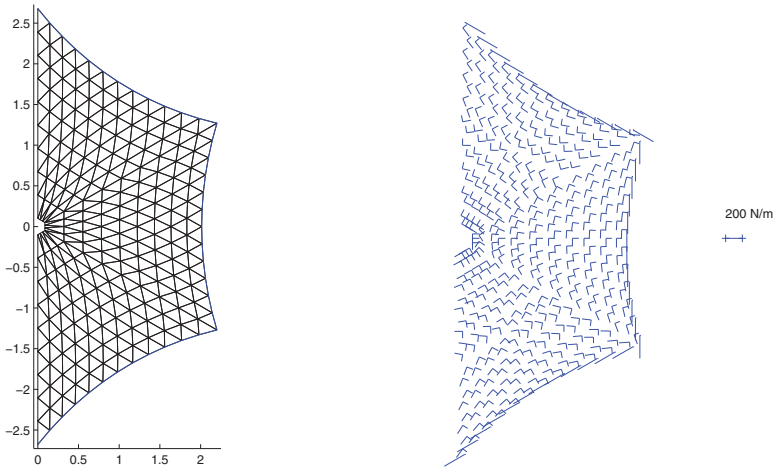

(a) 6 rib configuration

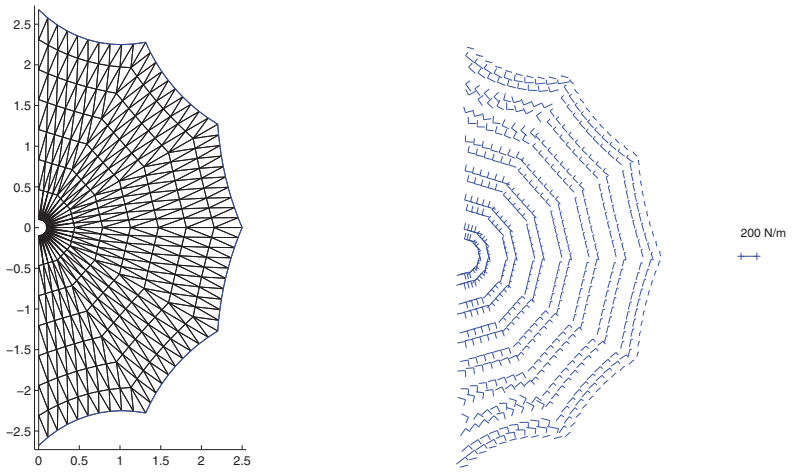

(b) 12 rib configuration

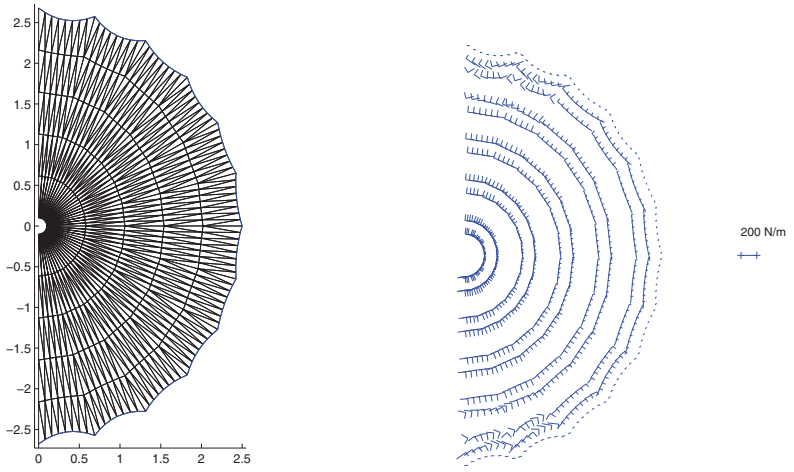

(c) 24 rib configuration

Figure 5.6: Shape and stress distributions of equilibrium shape of 5 m reflector with fixed boundary conditions.

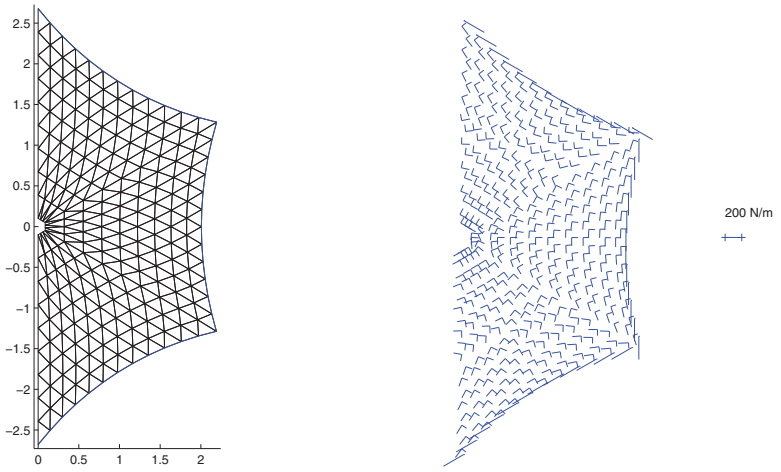

(a) 6 rib configuration

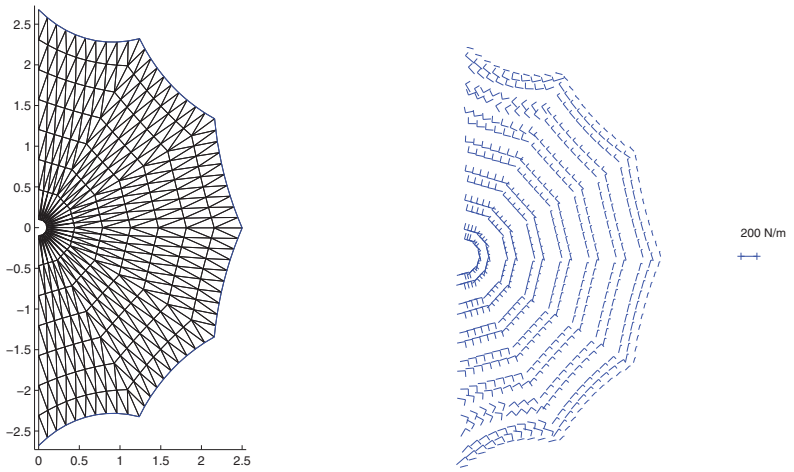

(b) 12 rib configuration

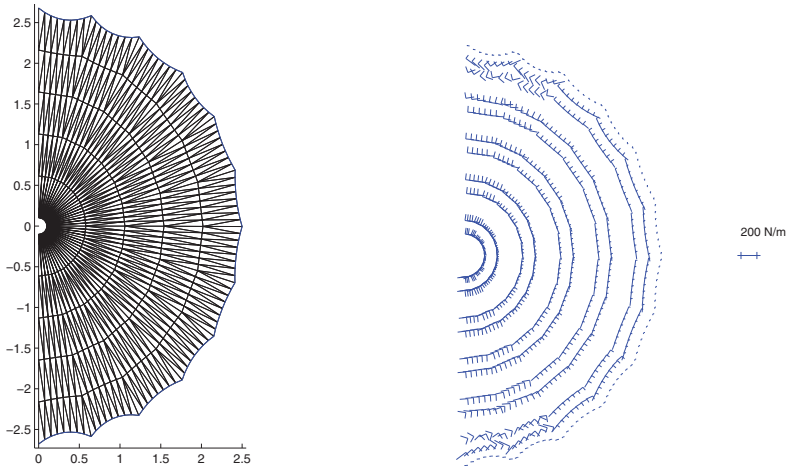

(c) 24 rib configuration

Figure 5.7: Shape and stress distributions of equilibrium shape of 5 m reflector with sliding $\perp$ boundary conditions.

5.5 10 m Reflector

The rms error of the reference surface and the equilibrium surface of 10 m offset reflectors are listed in Table 5.13. Table 5.14 lists the in-plane and out-of-plane rib loads applied by the equilibrium surface. Figures 5.8 and 5.9 show the equilibrium shapes and the principal stress distributions in reflectors with different numbers of ribs, for fixed and sliding $\perp$ boundary conditions, respectively.

No pictures are shown for the reflector with 36 ribs, as a sufficiently clear pattern emerges from the cases shown.

Table 5.15 lists the values of the maximum ratio between principal stresses in the 4 configurations that have been analysed. Note that this maximum ratio tends to occur about 90° from the plane of symmetry of the reflector; hence, this is the region where the formation of wrinkles is most likely.

Configuration	Reference surface	Boundary condition	Equilibrium surface
6 ribs	49.3	Fixed	51.6
		Slide $\perp$	51.5
12 ribs	13.5	Fixed	16.4
		Slide $\perp$	16.3
24 ribs	3.6	Fixed	5.0
		Slide $\perp$	5.1
36 ribs	1.6	Fixed	2.4
		Slide $\perp$	2.7

Table 5.13: Rms errors of 10 m diameter offset reflectors [mm].

Configuration	b.c.	Rib	Intermediate		Tip	
			out-plane	in-plane	out-plane	in-plane
6 ribs	Fixed	1	0.00	46.61	0.00	913.84
		2	1.03	45.23	11.31	837.15
		3	1.39	48.37	13.96	836.81
		4	0.00	54.11	0.00	913.30
	Slide $\perp$	1	0.00	46.22	0.00	910.25
		2	0.00	45.57	0.00	839.72
		3	0.00	48.62	0.00	838.73
		4	0.00	53.61	0.00	908.50
12 ribs	Fixed	1	0.00	36.57	0.00	301.59
		2	1.62	37.90	25.79	244.40
		3	0.88	51.07	16.21	152.72
		4	0.19	54.66	0.36	119.01
		5	0.66	51.72	16.98	152.72
		6	1.67	40.50	26.44	244.49
		7	0.00	40.79	0.00	301.74
	Slide $\perp$	1	0.00	34.40	0.00	292.31
		2	0.00	36.32	0.00	240.48
		3	0.00	52.95	0.00	157.57
		4	0.00	57.45	0.00	127.49
		5	0.00	53.40	0.00	157.33
		6	0.00	38.74	0.00	240.17
		7	0.00	38.53	0.00	292.00
24 ribs	Fixed	1	0.00	18.49	0.00	138.10
		2	0.67	18.29	3.95	137.43
		3	6.52	20.43	16.61	109.15
		4	2.61	22.94	4.06	78.83
		5	4.60	29.96	11.01	61.92
		6	1.81	31.48	1.00	45.10
		7	0.11	31.00	0.19	44.77
		8	1.97	31.60	1.36	45.11
		9	4.52	30.37	11.40	62.00
		10	2.66	23.79	4.42	78.88
		11	6.57	22.28	16.92	109.34
		12	0.67	21.37	4.14	137.61
		13	0.00	21.72	0.00	138.29
	Slide $\perp$	1	0.00	17.47	0.00	135.19
		2	0.00	17.26	0.00	134.42
		3	0.00	19.67	0.00	108.08
		4	0.00	22.95	0.00	79.01
		5	0.00	30.64	0.00	63.48
		6	0.00	32.09	0.00	47.87
		7	0.00	32.20	0.00	47.41
		8	0.00	32.14	0.00	47.82
		9	0.00	30.92	0.00	63.49
		10	0.00	23.62	0.00	78.92
		11	0.00	21.35	0.00	108.13
		12	0.00	20.39	0.00	134.43
		13	0.00	20.73	0.00	135.21

Table 5.14: Rib loads for 10 m diameter reflectors [N]. Table continued on next page.

Configuration	b.c.	Rib	Intermediate		Tip	
			out-plane	in-plane	out-plane	in-plane
36 ribs	Fixed	1	0.00	11.64	0.00	92.89
		2	0.31	11.58	2.75	92.56
		3	0.56	11.42	4.78	91.70
		4	7.79	14.06	11.83	72.65
		5	1.78	15.05	3.86	51.40
		6	1.65	14.37	3.39	50.49
		7	5.88	20.79	8.04	39.60
		8	1.64	21.16	1.17	28.14
		9	0.82	20.71	0.53	27.86
		10	0.07	20.57	0.13	27.76
		11	0.92	20.76	0.78	27.86
		12	1.74	21.27	1.40	28.15
		13	5.83	21.09	8.30	39.67
		14	1.69	14.93	3.67	50.51
		15	1.82	15.73	4.09	51.43
		16	7.83	15.36	12.03	72.79
		17	0.57	13.68	4.94	91.77
		18	0.31	13.99	2.83	92.64
		19	0.00	14.05	0.00	92.97
	Slide $\perp$	1	0.00	11.25	0.00	91.07
		2	0.00	11.15	0.00	90.84
		3	0.00	10.91	0.00	90.10
		4	0.00	13.61	0.00	72.13
		5	0.00	14.45	0.00	51.58
		6	0.00	14.90	0.00	50.60
		7	0.00	21.19	0.00	40.54
		8	0.00	21.17	0.00	29.66
		9	0.00	21.27	0.00	29.33
		10	0.00	21.32	0.00	29.22
		11	0.00	21.30	0.00	29.32
		12	0.00	21.22	0.00	29.63
		13	0.00	21.39	0.00	40.58
		14	0.00	15.34	0.00	50.54
		15	0.00	15.01	0.00	51.52
		16	0.00	14.78	0.00	72.19
		17	0.00	13.22	0.00	90.09
		18	0.00	13.56	0.00	90.83
		19	0.00	13.70	0.00	91.06

Continued from previous page.

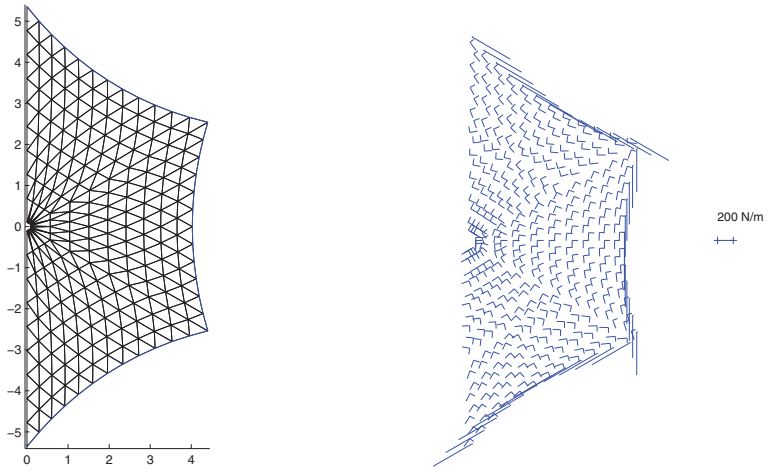

(a) 6 rib configuration

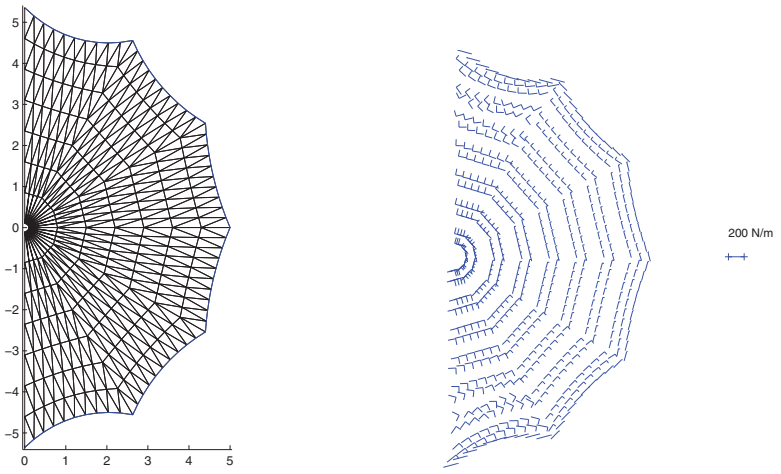

(b) 12 rib configuration

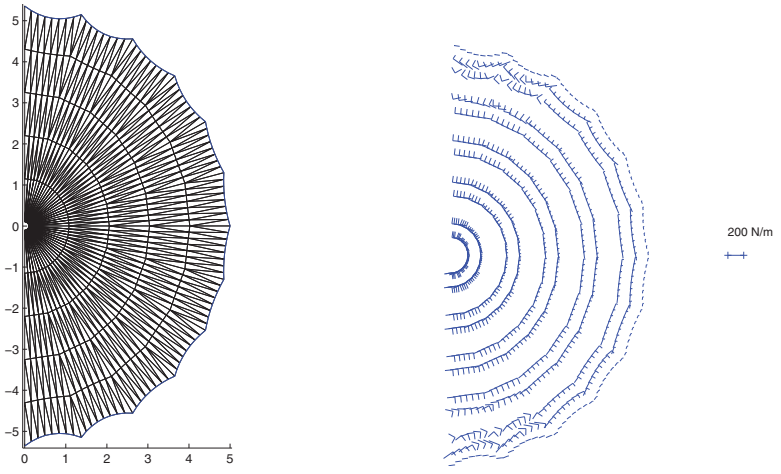

(c) 24 rib configuration

Figure 5.8: Shape and stress distributions of equilibrium shape of 10 m reflectors with fixed boundary conditions.

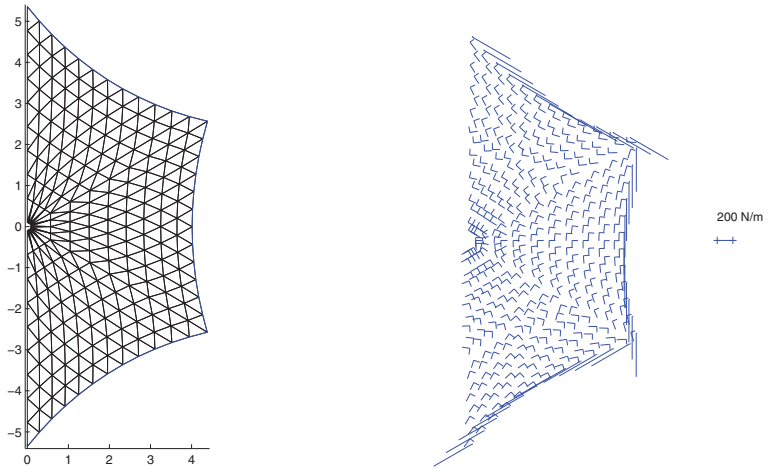

(a) 6 rib configuration

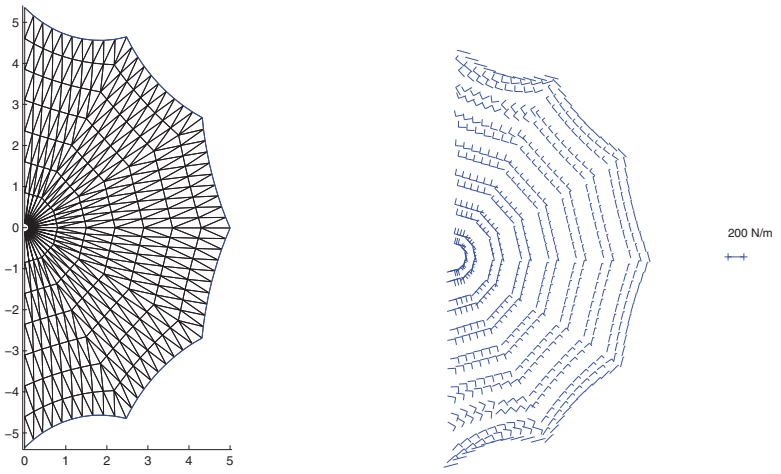

(b) 12 rib configuration

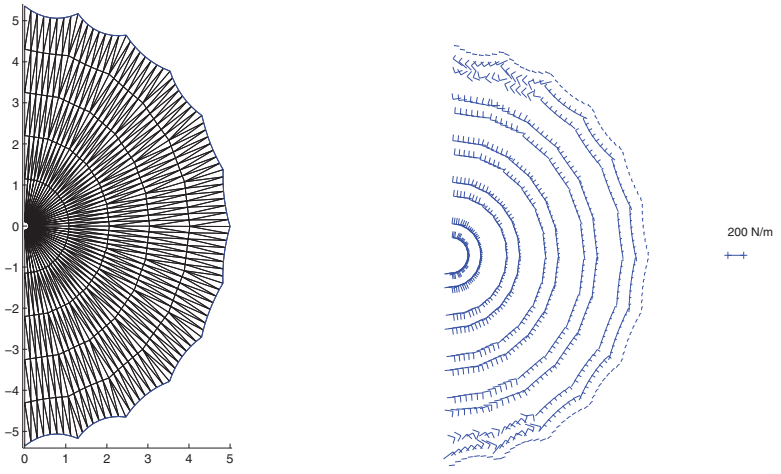

(c) 24 rib configuration

Figure 5.9: Shape and stress distributions of equilibrium shape of 10 m reflectors with sliding $\perp$ boundary conditions.

Configuration	b.c.	Max stress ratio
6 ribs	Fixed	2.06
	Slide $\perp$	2.12
12 ribs	Fixed	5.08
	Slide $\perp$	5.85
24 ribs	Fixed	4.31
	Slide $\perp$	5.30
36 ribs	Fixed	4.15
	Slide $\perp$	5.03

Table 5.15: Maximum stress ratio in reflector with D = 10 m

5.6 Summary and Discussion

Table 5.16 summarises the values of the rms errors of the reference and equilibrium surfaces for all of the configurations that have been analysed. It is instructive to compare these results with the symmetric reflectors that were analysed in our previous report (Lai, You and Pellegrino 1997) and shown in Table 5.17. The comparison shows that the rms errors for the offset configurations are about 30% worse than for the symmetric configuration. No doubt, the particular numerical value that we have found is related to the particular value of $F/D = 0.78$ that we have considered. Different values of F/D will be considered in Chapter 6.

Also, we have noticed that the magnitude of the in-plane forces on the ribs is close to the forces calculated in the symmetric case, whereas the out-of-plane loading has been made equal to zero in the offset reflector (just as in the symmetric reflector) by using boundary conditions that allow sliding in the direction $\perp$ to the plane of the ribs. Therefore, two-dimensionally curved ribs can still be used, making the manufacturing of the ribs much easier.

Finally, note that the results obtained in this chapter show that both the rms errors and the rib loading in offset reflectors increase linearly with the diameter of the reflector, hence key properties of reflector of any size can be estimated simply by scaling the results for a reference case (for this reason, a larger set of results have been presented the case D = 10 m). The same observation was made for symmetric reflectors.

Diameter	Configuration	Reference surface	Boundary condition	Equilibrium surface
1 m	6 ribs	4.8	Fixed	5.1
			Slide $\perp$	5.1
	12 ribs	1.3	Fixed	1.6
			Slide $\perp$	1.6
	24 ribs	0.3	Fixed	0.5
			Slide $\perp$	0.5
3 m	6 ribs	14.7	Fixed	15.4
			Slide $\perp$	15.4
	12 ribs	4.0	Fixed	4.9
			Slide $\perp$	4.9
	24 ribs	1.1	Fixed	1.5
			Slide $\perp$	1.5
5 m	6 ribs	24.6	Fixed	25.7
			Slide $\perp$	25.7
	12 ribs	6.7	Fixed	8.2
			Slide $\perp$	8.1
	24 ribs	1.8	Fixed	2.5
			Slide $\perp$	2.6
10 m	6 ribs	49.3	Fixed	51.6
			Slide $\perp$	51.5
	12 ribs	13.5	Fixed	16.4
			Slide $\perp$	16.3
	24 ribs	3.6	Fixed	5.0
			Slide $\perp$	5.1
	36 ribs	1.6	Fixed	2.4
			Slide $\perp$	2.7

Table 5.16: Rms errors of offset reflectors with different diameters [mm] and $F/D = 0.78$.

Diameter (m)	Configuration	Reference surface	Equilibrium surface
1	6 ribs	3.0	3.5
	12 ribs	0.9	1.3
	24 ribs	0.4	0.4
3	6 ribs	8.8	10.5
	12 ribs	2.6	3.9
	24 ribs	0.7	1.2
5	6 ribs	14.7	17.5
	12 ribs	4.3	6.6
	24 ribs	1.1	2.0
10	6 ribs	29.3	35.1
	12 ribs	8.6	13.1
	24 ribs	2.2	3.9

Table 5.17: Rms errors of *symmetric* reflectors [mm] with $F/D = 0.78$, for comparison with Table 5.16.

Chapter 6

An Alternative Configuration

In Section 5.1, we have pointed out that in CRTS reflectors with standard or central hub configurations there is a tendency for the prestress to become purely in the hoop direction in the gores that are furthest away from the plane of symmetry. There are two ways of addressing this problem. The approach that was adopted in Chapter 5 was to compute the initial prestress considering fewer ribs than their actual number. This cured the problem, to a certain extent, but at the expense of producing a rather uneven initial prestress along the surface of the reflector.

The alternative, which will be presented in this chapter, is to adopt the so-called *circular configuration*, introduced in Section 2.4.

Because the projection of a circular configuration reflector onto the local $X_L Y_L$ plane is a circle, the projections of all the gores will be identical. Thus, because the initial prestress distribution in the reflector is computed by considering only equilibrium in this plane, it will be uniform.

Out-of-plane equilibrium conditions are imposed during form-finding, but it will be shown that they cause only small changes in the prestress distribution. Hence, the final prestress distribution obtained by this approach will be almost uniform.

6.1 10 m Reflector

Results will be presented only for a 10 m diameter reflector with 24 ribs, as we know from Chapter 5 how to scale these results to reflectors with different diameters; 24 ribs is likely to be close to the number that would be selected for practical applications.

Figure 6.1 shows the initial prestress distribution obtained for $t_x = 80$ N/m and $t_y = 100$ N/m. The value of the cord tension is set to be such that the sag is $s = D/10$, which requires $T = 58.6$ N. Note that the corresponding T/D value is 5.86 N/m. Figure 6.1 clearly shows that in the circular configuration it is possible to achieve a much more even biaxial stress distribution than with the standard and central hub configurations. Therefore, smaller out-of-plane loading on the ribs and a smaller ratio between the highest and lowest principal stress can be

expected in the equilibrium configuration.

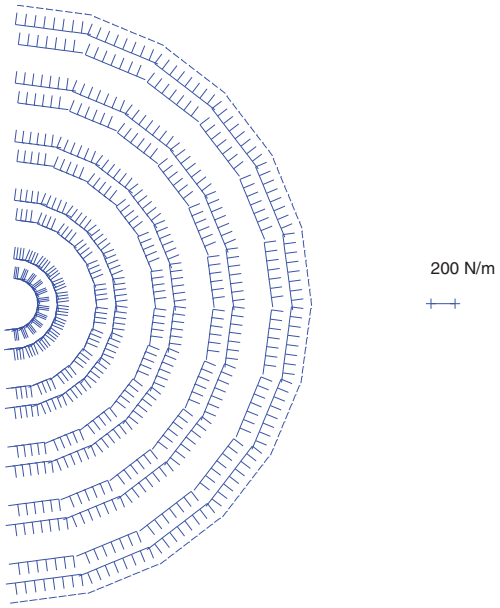

Figure 6.1: Initial stress distribution.

The rms error of the reference surface and the equilibrium surface are shown in Table 6.1. Table 6.2 lists the in-plane and out-of-plane loads applied by the equilibrium surface onto the ribs. Figure 6.2 shows the equilibrium shapes of the reflector for the two different types of boundary conditions, and the corresponding principal stress distribution.

Configuration	Reference surface	Boundary condition	Equilibrium surface
24 ribs	3.3	Fixed	5.1
		Slide $\perp$	5.1

Table 6.1: Rms errors of 10 m diameter reflectors with circular configuration [mm].

Configuration	b.c.	Rib	Intermediate		Tip	
			out-plane	in-plane	out-plane	in-plane
24 ribs	Fixed	1	0.00	16.47	0.00	127.45
		2	0.09	16.50	0.22	127.46
		3	0.16	16.60	0.42	127.49
		4	0.20	16.76	0.57	127.54
		5	0.21	16.99	0.63	127.60
		6	0.17	17.26	0.57	127.64
		7	0.10	17.57	0.39	127.67
		8	0.02	17.91	0.15	127.68
		9	0.07	18.25	0.08	127.67
		10	0.12	18.57	0.22	127.65
		11	0.12	18.82	0.24	127.61
		12	0.07	18.99	0.15	127.58
		13	0.00	19.05	0.00	127.57
	Slide $\perp$	1	0.00	16.50	0.00	127.56
		2	0.00	16.53	0.00	127.57
		3	0.00	16.62	0.00	127.58
		4	0.00	16.77	0.00	127.60
		5	0.00	16.98	0.00	127.60
		6	0.00	17.24	0.00	127.60
		7	0.00	17.55	0.00	127.59
		8	0.00	17.89	0.00	127.59
		9	0.00	18.23	0.00	127.59
		10	0.00	18.56	0.00	127.60
		11	0.00	18.83	0.00	127.60
		12	0.00	19.01	0.00	127.60
		13	0.00	19.07	0.00	127.60

Table 6.2: Rib loads for 10 m diameter reflectors with circular configuration [N].

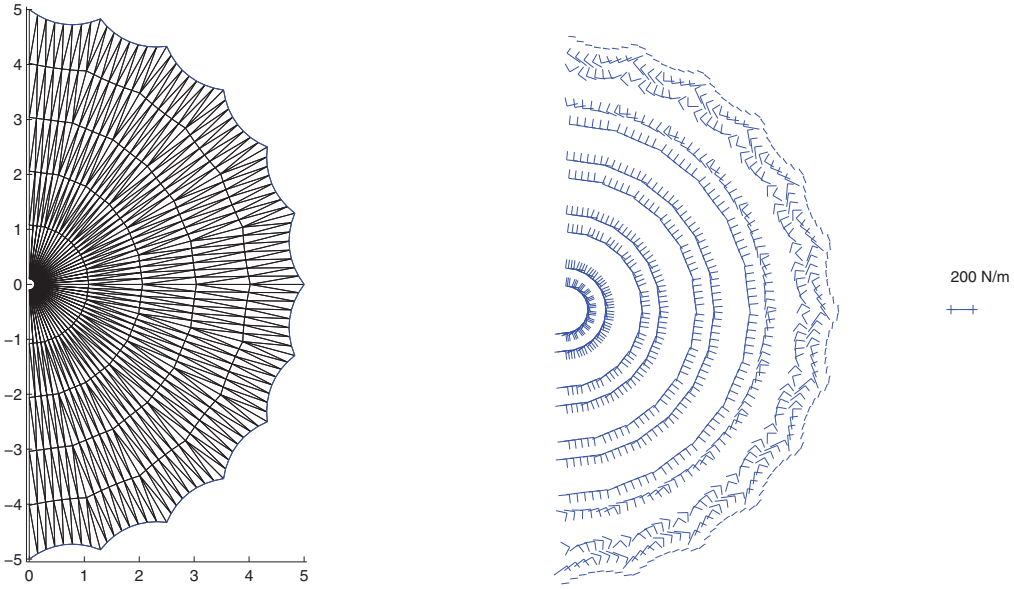

(a) Fixed rib boundary

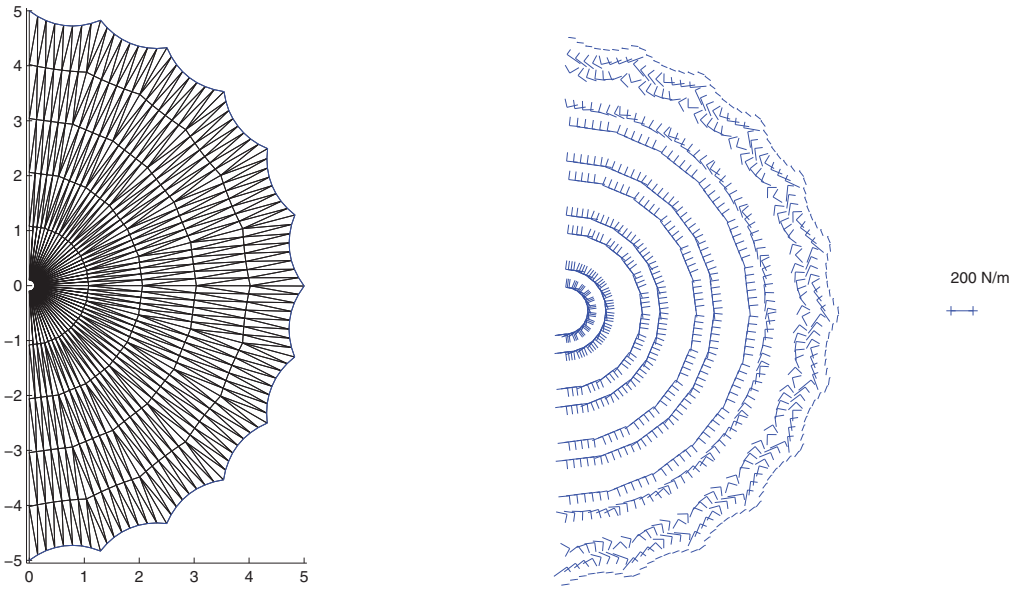

(b) Sliding $\perp$ boundary

Figure 6.2: Shape and stress distributions of equilibrium shape of 10 m reflectors with 24 ribs.

6.2 Reflectors with different F/D ratios

Until now, we have considered only reflectors with a particular value of $F/D = 0.78$. Since an extensive study of the effects of varying F/D in CRTS reflectors would be beyond the scope of the present work, in this section we present estimates for the rms error of reflectors with four different F/D ratios: 0.25, 0.50, 0.75 and 1.00. From these estimates one can get a feel for the way in which the value of F/D affects the surface accuracy of a reflector.

Because the circular configuration appears to offer the best combination of stress distribution and surface accuracy, all results that are presented are for a 10 m diameter with 24 ribs, as in the previous section, with circular configuration.

Table 6.3 lists the rms error of the reference surface and the equilibrium surface for the four F/D ratios. Table 6.4 shows the maximum stress ratios that are obtained.

Tables 6.5- 6.8 list the in-plane and out-of-plane rib loads applied by equilibrium surface. They show that the higher F/D, the more accurate the shape and the lower the rib loading. This result can be explained as follows. Since higher values of F/D mean that the reflector is flatter, see fig. 6.3, there is less geometrical distortion during form-finding, because the initial in-plane stress distribution is almost in equilibrium in 3D. Note, though, that the biaxial stress distribution at equilibrium is hardly affected by F/D, see fig. 6.4.

F/D	Reference surface	Boundary condition	Equilibrium surface
0.25	5.0	Fixed	7.6
		Slide $\perp$	7.4
0.50	4.3	Fixed	6.7
		Slide $\perp$	6.6
0.75	3.4	Fixed	5.3
		Slide $\perp$	5.3
1.00	2.7	Fixed	4.2
		Slide $\perp$	4.2

Table 6.3: Variation of rms error with F/D [mm] for D = 10 m and 24 ribs.

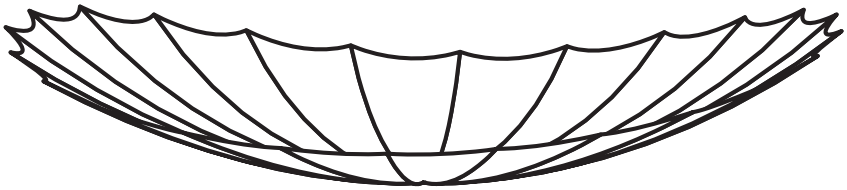

(a) $F/D = 0.25$

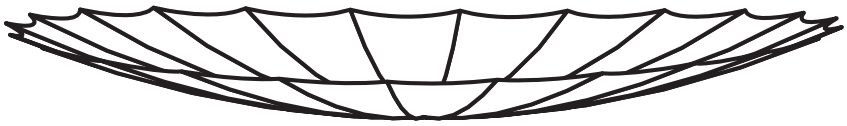

(b) $F/D = 0.50$

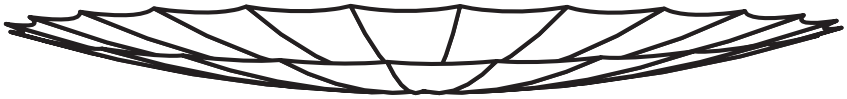

(c) $F/D = 0.75$

(d) $F/D = 1.00$

Figure 6.3: 3D view of equilibrium surface of reflectors (D = 10 m, 24 ribs) with different F/D ratios.

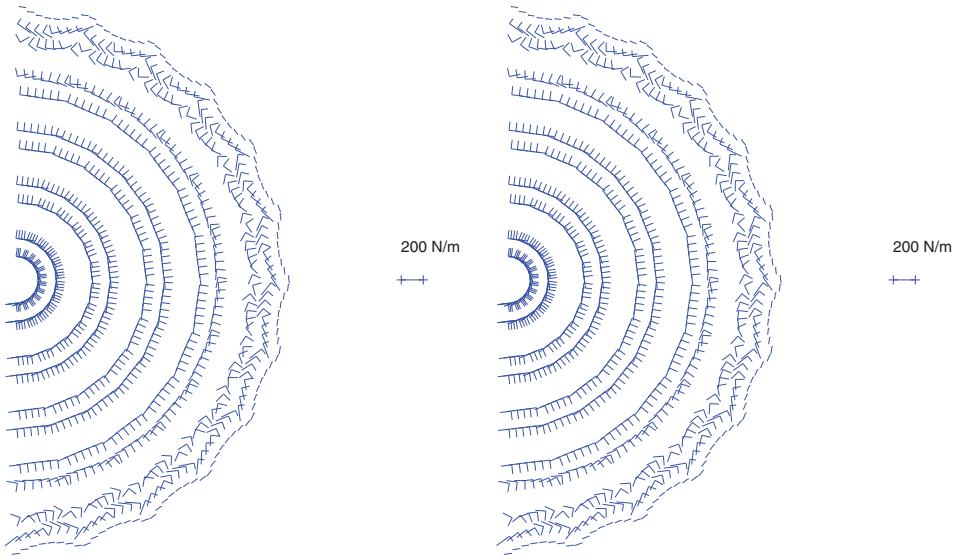

(a) $F/D = 0.25$ (b) $F/D = 0.50$

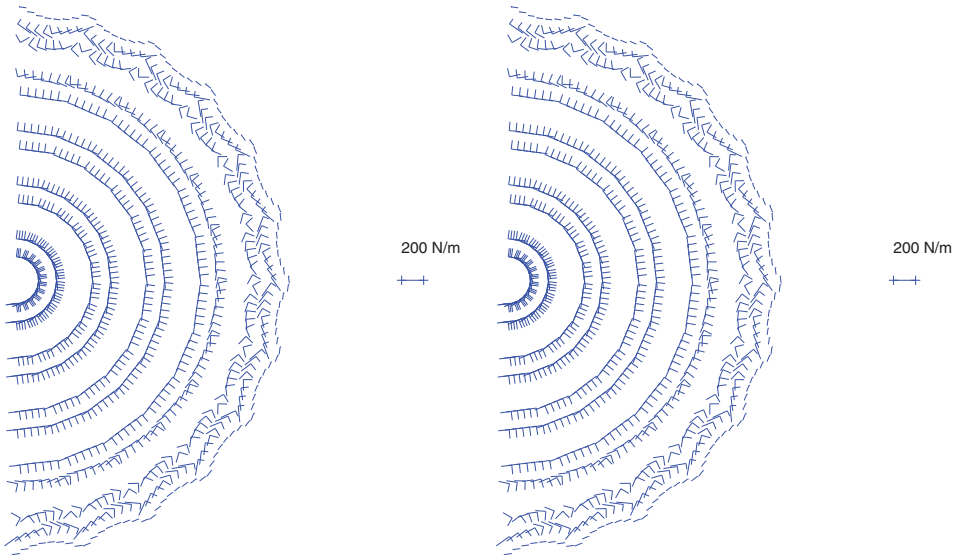

(c) $F/D = 0.75$ (d) $F/D = 1.00$

Figure 6.4: Final stress distribution of reflectors (D = 10 m, 24 ribs) with different F/D values.

F/D	b.c.	Max stress ratio
0.25	Fixed	2.71
	Slide $\perp$	2.90
0.50	Fixed	2.68
	Slide $\perp$	2.72
0.75	Fixed	2.68
	Slide $\perp$	2.70
0.78	Fixed	2.68
	Slide $\perp$	2.69
1.00	Fixed	2.69
	Slide $\perp$	2.69

Table 6.4: Maximum stress ratios in reflectors (D = 10 m, 24 ribs) with different F/D values.

6.3 Discussion

Although only reflectors with one particular diameter and number of ribs have been considered, it has been clearly shown that the circular configuration leads to a superior stress distribution and uniform loading of all ribs. The maximum stress ratio in the surface at equilibrium is less than 3, which means that the formation of wrinkles is very unlikely. The surface accuracy is about the same as for the central hub configuration.

Another advantage of the circular configuration is that no special computations are required to determine the initial prestress distribution, as one can choose the prestress in one gore and all other gores have identical stress components.

A preliminary study of the variation of the rms error of CRTS reflectors with F/D has shown that the change in the equilibrium surface error is proportional to the error of the reference surface. The final stress distribution and the rib loads are not affected much by the variation of F/D.

b.c.	Rib	Intermediate		Tip	
		out-plane	in-plane	out-plane	in-plane
Fixed	1	0.00	21.07	0.00	127.38
	2	0.99	21.24	1.17	127.61
	3	1.86	21.74	3.09	128.21
	4	2.49	22.60	5.93	128.95
	5	2.76	23.86	8.87	129.61
	6	2.51	25.61	10.34	130.10
	7	1.59	27.89	8.62	130.54
	8	0.32	30.63	3.09	130.98
	9	2.03	33.58	4.32	131.12
	10	3.57	36.50	9.35	130.59
	11	3.96	39.20	9.01	129.45
	12	2.68	41.34	4.81	128.17
	13	0.00	42.21	0.00	127.59
Slide $\perp$	1	0.00	21.31	0.00	128.33
	2	0.00	21.49	0.00	128.67
	3	0.00	22.04	0.00	129.47
	4	0.00	22.88	0.00	130.27
	5	0.00	23.99	0.00	130.55
	6	0.00	25.44	0.00	130.09
	7	0.00	27.39	0.00	129.30
	8	0.00	29.93	0.00	128.86
	9	0.00	32.94	0.00	129.09
	10	0.00	36.15	0.00	129.64
	11	0.00	39.19	0.00	129.83
	12	0.00	41.51	0.00	129.35
	13	0.00	42.42	0.00	128.99

Table 6.5: Rib loads for reflectors (D = 10 m, 24 ribs) with $F/D = 0.25$ [N].

b.c.	Rib	Intermediate		Tip	
		out-plane	in-plane	out-plane	in-plane
Fixed	1	0.00	18.56	0.00	127.41
	2	0.29	18.63	0.60	127.46
	3	0.53	18.87	1.23	127.59
	4	0.68	19.25	1.82	127.75
	5	0.72	19.79	2.21	127.93
	6	0.61	20.48	2.17	128.08
	7	0.37	21.31	1.59	128.18
	8	0.07	22.26	0.59	128.23
	9	0.31	23.27	0.45	128.20
	10	0.53	24.25	1.12	129.09
	11	0.56	25.10	1.18	127.93
	12	0.36	25.68	0.72	127.78
	13	0.00	25.89	0.00	127.72
Slide $\perp$	1	0.00	18.65	0.00	127.76
	2	0.00	18.72	0.00	127.80
	3	0.00	18.94	0.00	127.90
	4	0.00	19.30	0.00	127.99
	5	0.00	19.79	0.00	128.02
	6	0.00	20.43	0.00	127.98
	7	0.00	21.22	0.00	127.90
	8	0.00	22.15	0.00	127.86
	9	0.00	23.18	0.00	127.87
	10	0.00	24.21	0.00	127.90
	11	0.00	25.11	0.00	127.91
	12	0.00	25.73	0.00	127.89
	13	0.00	25.95	0.00	127.87

Table 6.6: Rib loads for reflectors (D = 10 m, 24 ribs) with $F/D = 0.50$ [N].

b.c.	Rib	Intermediate		Tip	
		out-plane	in-plane	out-plane	in-plane
Fixed	1	0.00	16.66	0.00	127.45
	2	0.10	16.70	0.24	127.46
	3	0.18	16.81	0.47	127.50
	4	0.23	16.99	0.64	127.56
	5	0.23	17.23	0.71	127.61
	6	0.19	17.53	0.65	127.66
	7	0.11	17.88	0.45	127.70
	8	0.02	18.25	0.17	127.71
	9	0.08	18.63	0.09	127.70
	10	0.13	18.98	0.26	127.67
	11	0.14	19.27	0.28	127.63
	12	0.08	19.46	0.18	127.60
	13	0.00	19.53	0.00	127.59
Slide $\perp$	1	0.00	16.69	0.00	127.58
	2	0.00	16.73	0.00	127.58
	3	0.00	16.83	0.00	127.60
	4	0.00	17.00	0.00	127.62
	5	0.00	17.22	0.00	127.63
	6	0.00	17.51	0.00	127.62
	7	0.00	17.85	0.00	127.61
	8	0.00	18.22	0.00	127.61
	9	0.00	18.61	0.00	127.61
	10	0.00	18.97	0.00	127.62
	11	0.00	19.28	0.00	127.62
	12	0.00	19.48	0.00	127.62
	13	0.00	19.55	0.00	127.62

Table 6.7: Rib loads for reflectors (D = 10 m, 24 ribs) with $F/D = 0.75$ [N].

b.c.	Rib	Intermediate		Tip	
		out-plane	in-plane	out-plane	in-plane
Fixed	1	0.00	15.26	0.00	127.44
	2	0.04	15.28	0.11	127.44
	3	0.07	15.33	0.20	127.46
	4	0.09	15.42	0.26	127.48
	5	0.09	15.54	0.28	127.50
	6	0.07	15.68	0.24	127.52
	7	0.04	15.84	0.17	127.54
	8	0.01	16.01	0.06	127.54
	9	0.02	16.17	0.03	127.54
	10	0.05	16.32	0.09	127.53
	11	0.05	16.44	0.10	127.51
	12	0.03	16.52	0.06	127.50
	13	0.00	16.54	0.00	127.50
Slide $\perp$	1	0.00	15.28	0.00	127.49
	2	0.00	15.29	0.00	127.49
	3	0.00	15.34	0.00	127.50
	4	0.00	15.42	0.00	127.50
	5	0.00	15.54	0.00	127.50
	6	0.00	15.67	0.00	127.50
	7	0.00	15.83	0.00	127.50
	8	0.00	16.00	0.00	127.50
	9	0.00	16.17	0.00	127.50
	10	0.00	16.32	0.00	127.51
	11	0.00	16.44	0.00	127.51
	12	0.00	16.52	0.00	127.51
	13	0.00	16.55	0.00	127.51

Table 6.8: Rib loads for reflectors (D = 10 m, 24 ribs) with $F/D = 1.00$ [N].

Chapter 7

Conclusion

7.1 Discussion

Prior to the study presented in this report, there was concern over the applicability of the CRTS concept to offset reflectors. It was thought that setting up a prestressed membrane with asymmetric shape may well be impossible, unless one accepted very stiff ribs, able to carry the large out-of-plane loads resulting from the difference in prestress between adjacent gores.

Although the use of stiff ribs is still an option —but we think that it would run against the CRTS concept— we have found two different ways of designing offset reflectors whose membranes are properly stressed and yet apply only in-plane loads on the ribs.

The most conventional design, called central hub configuration, puts the centre of the hub at the point obtained by projecting the centre of the ellipse defined by the tips of the ribs onto the local plane $X_L Y_L$. To produce a successful design of this type, one has to choose a suitable initial prestress at the start of the form-finding process. Prestress distributions need to satisfy two-dimensional equilibrium, i.e. the prestress components in the plane $X_L Y_L$ need to be in equilibrium, at the gore-gore interfaces —as the ribs can carry only in-plane loading— and also at the gore-cord interfaces.

The most elegant and unexpected design solution, called circular configuration, has the special feature that the tips of the ribs are not co-planar. Instead, their projections onto the local plane $X_L Y_L$ lie on a circle. This greatly simplifies the choice of a suitable initial state of prestress because, as far as two-dimensional equilibrium is concerned, this configuration is "axi-symmetric" and hence adjacent gores are equally stressed.

Thus, it has been shown that CRTS reflectors with offset configuration are feasible, and extensive sets of results have been presented to aid the design of future reflectors. Finally, it should be pointed out that the results presented in this report are expected to be correct, because the approach from which they were obtained is an extension of the approach developed in Lai, You and Pellegrino (1997) —which was experimentally verified— but a direct experimental validation

has yet to be carried out. This will be done during the next phase of this study.

7.2 Summary of Results

The results obtained in this report can be divided into three categories, as follows.

7.2.1 Geometric configuration

Three different configurations of offset CRTS reflectors have been introduced, of which only two are obtained by intersecting the parent paraboloid with a circular cylinder parallel to the axis of the paraboloid. The rms errors of these configurations are comparable, and the main differences are in the associated prestress distribution.

The standard configuration, which has the hub centred on the axis of the circular cylinder, tends to produce the least biaxial distribution of prestress in the membrane. It is better suited to reflectors with stiff ribs, that can carry large out-of-plane loads.

The central hub configuration, which has the hub centre at the point obtained by projecting the centre of the ellipse obtained by intersecting the cylinder and the paraboloid onto the local plane $X_L Y_L$, can produce acceptable distributions of prestress.

The circular configuration, which is obtained by intersecting the paraboloid with a circular cylinder whose axis is parallel to the local axis Z_L, tends to produce the best distributions of prestress. Because in this configuration the shape of the reflecting membrane does not match the standard illumination pattern, it is likely that a part of the surface would not be fully utilised.

7.2.2 Shape and stress analysis

The shape and stress analysis algorithm that has been used for offset reflectors uses the same algorithms that were previously developed for symmetric reflectors. Because of the lower order of symmetry of offset reflectors, a *gore-by-gore design* will inevitably lead to large out-of-plane loading of the ribs, which will need to be much stiffer than assumed so far in the CRTS concept. This option poses no great theoretical problems, although there may be significant problems in designing ribs with the required properties.

As it is anticipated that the ribs will continue to be of the very flexible, collapsible type, a key aim of this study has been to find ways of producing *global designs* that reduce to zero the out-of-plane loading on the ribs.

The best way of achieving this in general is to ensure that any candidate state of prestress satisfies the condition that it is in equilibrium in a two-dimensional sense. This can be ensured in a relatively straightforward way, by doing simple preliminary computations. For reflectors with more than 12 ribs this preliminary

computation is done for a reduced number of ribs, to avoid excessive reduction of radial prestress in the gores that are furthest away from the plane of symmetry.

When three-dimensional equilibrium conditions are imposed, during the form-finding analysis that follows, it is best to use a boundary condition that allows sliding in the directions perpendicular to the plane of the ribs, at the connections between the membrane and the ribs.

7.2.3 Results

It has been shown that *the rms surface error of CRTS reflectors* ***with equal prestress levels*** *increases proportionally to their diameter, together with the forces applied to the ribs and the edge cords.*

Hence, one can get a clear picture by considering only one particular value of D, and the tables included in this section summarise four key sets of results. Table 7.1 compares rms errors in symmetric and offset reflectors (only one value is given for offset reflectors, as the different configurations give almost the same rms error). Table 7.2 shows the variation of the rms error with the ratio between focal length and diameter. Table 7.3 compares the "highest" ratios between maximum and minimum principal stresses for the best designs that have been produced during this study. Table 7.4 compares the maximum tip loads that are applied on the ribs, in symmetric and offset reflectors.

Ribs	Symmetric	Offset
6	35.1	51.5
12	13.1	16.3
24	3.9	5.1
36	-	2.7

Table 7.1: Rms errors [mm] of equilibrium surface of reflectors with $D = 10$ m, $A = 1$ m, and $F = 7.8$ m.

F/D	error
0.25	7.4
0.50	6.6
0.75	5.3
1.00	4.2

Table 7.2: Variation of rms error [mm] with F, for reflectors with $D = 10$ m, $A = 1$ m and 24 ribs.

Ribs	Configuration		
	Symmetric	Offset central hub	Offset circular
6	2.08	2.12	-
12	2.81	5.85	-
24	3.17	5.30	2.69
36	2.85	5.03	-

Table 7.3: Maximum stress ratio in reflectors with $D = 10$ m, $A = 1$ m, and $F = 7.8$ m.

Ribs	Configuration		
	Symmetric†	Offset central hub	Offset circular
6	1468	910	-
12	846	302	-
24	444	135	128
36	299	91	-

Table 7.4: Maximum tip loads on ribs [N] for reflectors with $D = 10$ m, $A = 1$ m, and $F = 7.8$ m († based on results obtained in Lai, You and Pellegrino (1997) for higher stress levels $\simeq 170$ N/m).

Bibliography

Fischer, A. (1994). Bending instabilities of thin-walled transversely curved metallic strips. CUED/D-STRUCT/TR154, University of Cambridge.

Lai, C. Y., You, Z. and Pellegrino, S. (1997). Shape and stress analysis of symmetric CRTS reflectors. CUED/D-STRUCT/TR170. University of Cambridge.

Levy, R. (1996). *Structural Engineering of Microwave Antennas*. IEEE Press.

Rits, W. J. (1996). A multipurpose deployable membrane reflector. *Esa Bulletin 88*, pp. 66-71.

Seffen, K. A. and Pellegrino, S. (1999). Deployment dynamics of tape springs. *Proceedings Royal Society of London*, Part A, Vol. 455, pp. 1003-1048.

Seffen, K. A., You, Z. and Pellegrino, S. (1997). Folding and deployment of curved tape springs. CUED/D-STRUCT/TR171, University of Cambridge.

You, Z. and Pellegrino, S. (1994). Study of the folding and deployment aspects of a Collapsible Rib Tensioned Surface (CRTS) Antenna reflector. CUED/D-STRUCT/TR144, University of Cambridge.